# NASA Contractor Report 165655



# EXPERIMENTAL INVESTIGATIONS ON THE V/STOL TUNNEL AT NASA/LANGLEY RESEARCH CENTER

P. Stephen Barna

P. STEPHEN BARNA, CONSULTANT
1049 N. Lexan Crescent
Norfolk, Virginia 23508



NASA Purchase Order L-12343B
February 1981



NASA
National Aeronautics and Space Administration
**Langley Research Center**
Hampton, Virginia 23665

TABLE OF CONTENTS



LIST OF TABLES

# EXPERIMENTAL INVESTIGATIONS ON THE V/STOL TUNNEL AT NASA/LANGLEY RESEARCH CENTER

By

P. Stephen Barna

## SUMMARY

Calibration of the V/STOL tunnel at NASA/Langley Research Center (LaRC) with the test section in the open and closed modes of operation was performed during the period from March 1978 to June 1980. During this period some time was first spent in designing a serviceable traverse mechanism and finding a suitable sensor that could be employed to measure both flow velocities and direction at any section of the tunnel circuit.

Most of the tests were performed with the tunnel operating at three different speeds. Except for the testing area, traverses were taken at all other sections considered to be relevant around the tunnel circuit for the discovery of the prevailing flow conditions during normal tunnel operations. Surveying the test Section was considered unnecessary at this time because the flow had been previously studied and found satisfactory except when the test area was open. Moreover, the determination of flow in the testing area did not fall within the scope of the investigations, which were aimed at establishing locations of unsatisfactory flow as a basis for future improvements.

The test results show that the flow around the tunnel circuit gradually deteriorated with increasing distance from the testing area. At the beginning of the circuit, the flow in the first diffuser was still satisfactory; at the end of the circuit, the flow approaching the contraction had become entirely unsatisfactory. Deterioration of flow was due largely to turning the stream around the corners, with the resulting flow distortion affecting the diffusers downstream. The large end of the diffuser was found stalled on one side, and nearly stalled flow was also found

at the tip of the fan. Cumulatively these adverse flow characteristics were found to reduce the efficiency of the tunnel performance.

## INTRODUCTION

The calibration of full-scale wind tunnels is an accepted standard procedure which usually calls for the evaluation of flow conditions. A relatively simple evaluation concerns only the test section of the tunnel. At times, however, a need also arises for probing the flow conditions at other sections as well-occasionally even around the entire tunnel circuit. This is so because it has been found that most of the flow patterns around the tunnel circuit have markedly digressed from the "ideal" assumed flow pattern upon which the original design was based.

Experience teaches us that tunnel flow separation problems usually occur in the diffuser after the fan. It is a well-known fact that, once the flow separates from the diffuser wall, the resulting fluctuations downstream become noticeable, affecting both the flow in the test section and the tunnel performance.

Recent studies on diffusers indicate that performance expressed in pressure recovery depends on the flow "quality" at inlet to the diffuser in addition to its geometry. Under quality comes, first, blockage at inlet, which is closely linked to velocity distribution. Effects of viscosity come second (Reynolds number at inlet), and turbulence level comes third. Any other type of disturbance, such as a nacelle protruding into the diffuser or the diffuser changing cross-sectional configuration, adds to the complexity of the flow.

Since closed-circuit wind tunnels repeatedly turn around approximately the same air quantity, it is then the "history" of the flow that needs further consideration. This means that each component (corners, diffusers, etc.) of the tunnel through which the air passes affects the successive components downstream. Therefore, each component's performance, in addition to its design, is influenced by the flow conditions upstream.

Design and performance data available on components (corners, diffusers, etc.) are the results of tests which were most probably performed under a variety of flow conditions which were nevertheless termed "ideal." For example, published results on the flow around a bend assume uniform velocity distribution right across the flow upstream. However, the flow even upstream of the first corner in a wind tunnel cannot be uniform right across because of the buildup of boundary layer along the preceding diffuser, which reduces the width of the uniform flow. Since the corner has to turn uniform as well as nonuniform flow (near the walls), it would be unreasonable to expect a completely uniform flow to emerge on the downstream side. Furthermore, if the duct downstream from the first corner is a diffuser, an additional boundary-layer buildup is experienced, and the uniformity of flow becomes further impaired. Consequently, the flow after the corner may altogether become nonuniform. It may even become asymmetric as well, owing to the fact that, in the process of turning, flows generally develop a pressure gradient across the stream, the higher pressure being on the outer side to balance centrifugal forces. Downstream from the corner, during the process of pressure equalization, parts of the stream run ahead, which explains why the flow becomes neither uniform nor axisymmetric. Should the fan be located downstream from the second corner, it may reasonably be anticipated that the velocity distribution in the flow annulus will neither be uniform nor symmetric.

For axial flow fans with fixed blade settings, however, there is no provision to compensate for asymmetric through-flow conditions, which result in a flow that is asymmetric downstream from the fan.

The large diffuser (following the fan) suffers from the disadvantage of receiving a turbulent and nonuniform flow from the fan, thus preventing the diffuser from performing satisfactorily. In transit through the diffuser the flow profile further deteriorates. Since the third and fourth corners are considered incapable of restoring uniformity to flow, the contraction upstream from the test section can improve the flow to

a limited extent and only if the contraction ratio is large. It cannot reduce the prevailing turbulence to the level anticipated by its geometry because of the nonuniform flow distribution at entry. As a result, the turbulence level in the test section is also higher than the desired level, and so the first diffuser downstream from the test section may be affected.

Ultimately, the operation of the wind tunnel depends on the performance of its components. This in turn depends on the history of the flow, the starting point for which may be the velocity distribution in the test section and possibly the prevailing turbulence level therein.

## SYMBOLS

| | |
|---|---|
| $C_p$ | pressure coefficient defined in text |
| $C_L$ | lift coefficient |
| $C_D$ | drag coefficient |
| C | chord of fan blade at location r, m |
| f | frequency, Hz |
| g | gravitational acceleration, $m/sec^2$ |
| $H_E$ | Euler "lift" defined as $\Delta p/\rho g$, m |
| K | lift/drag ratio |
| n | rotational speed of fan, rpm |
| J | advance ratio $V_a/V_t$ |
| p | static pressure at any point of surface, Pa |
| $p_1, p_3$ | static pressure at side port of yaw tube, Pa |
| $p_2$ | pressure at the center port, Pa |

| | |
|---|---|
| $p_\infty$ | static pressure of approaching flow, Pa |
| $\Delta p_t$ | total pressure rise across the fan, Pa |
| $p_E$ | Euler pressure rise across fan, Pa |
| $q_r$ | dynamic pressure ratio defined as $q/q_{max}$, $q_{max}$ = 100 lb/ ft$^2$ in the test section |
| q | dynamic head $1/2\rho V^2$, Pa |
| $Q_p$ | defined as $p_2 - 1/2\ (p_1 + p_3)$ |
| r | radius along fan blade, m |
| R | tip radius of fan, m |
| $R_e$ | Reynolds number based on tube diameter, $R_e = Vd/\nu$ |
| t | plane of fan rotation |
| u | velocity of airstream at y distance from inner wall, m/s |
| $U_{max}$ | maximum velocity attained at any cross section, m/s |
| $U_1$ | relative velocity at blade leading edge, m/s |
| $U_2$ | relative velocity at blade trailing edge, m/s |
| $U_m$ | mean relative velocity $(U_1 + U_2)/2$, m/s |
| $U_\infty$ | approach velocity towards cylinder, m/s |
| $V_a$ | axial flow through the fan at r location, m/s |
| $V_t$ | tangential speed of fan blade at r location |
| $V_o$ | absolute velocity of air downstream from fan, m/s |
| $V_w$ | whirl velocity downstream from fan, m/s |
| y | distance from inner wall |
| w | width of the tunnel |

$\alpha_m$ angle of incidence of blade element with $U_m$, degree

$\omega$ angular rotational speed of fan, $sec^{-1}$

$\beta_m$ angle of mean relative velocity of flow through fan blade, degree

$\theta$ angle enclosed between central port and airstream (yaw tube)

$\phi$ angle of airstream downstream from fan enclosed with axial direction

$\sigma$ radius ratio r/R

$\rho$ air density, $kg/m^3$

$\eta$ blade element efficiency

$\gamma$ profile setting angle of the blade, degree

$\delta$ presetting angle of yaw tube, degree

T.S. traverse station

## BRIEF DESCRIPTION OF THE V/STOL TUNNEL COMPONENTS

In order to make recognizable the characteristic features of the V/Stol tunnel, the circuit will be briefly reviewed. The various components are noted on figure 1, which shows the plan view of the tunnel. Table 1 gives the relevant details of these components.

The test section is followed by the first diffuser, which is provided with air intake flaps that can be operated open, closed, or at any setting in between. At the end of the first diffuser is the first corner, provided with equally spaced turning vanes, which is followed by the second diffuser. The flow control vanes, placed into the second diffuser, provide better speed control at very low test section velocities. A large mesh

wire screen is fitted over the entire area of the second corner to prevent large pieces of debris from getting into the fan. The second corner is followed by the third diffuser, designed for transition from a rectangular cross section to a circular cross section. The axial flow fan is located in a cylindrical shell and is fitted with a nacelle that protrudes into the large fourth diffuser, which is designed for transition from a circular to a rectangular cross section. The air exhaust is located at the end of the fourth diffuser. The third and fourth corners are connected with a rectangular duct of constant cross section. Finally, the contraction closes the return circuit. A set of two screens is fitted over the entire cross section at inlet to the contraction. Note that neither the rectangular section of the testing section nor any of the other components with rectangular sections was provided with corner fillets.

Table 1. Approximate cross-sectional area of components.

| Component | Inlet Area $m^2$ | Inlet Area $ft^2$ | Outlet Area $m^2$ | Outlet Area $ft^2$ | Area Ratio Outlet/Inlet |
|---|---|---|---|---|---|
| Contraction | 263.5 | 2835.75 | 29.3 | 315.4 | 1:8.99 |
| Test section | 29.3 | 315.4 | 32.8 | 353.5 | 1.12:1 |
| First diffuser | 32.8 | 353.5 | 79.0 | 850.5 | 2.41:1 |
| Second diffuser | 79.0 | 850.5 | 98.3 | 1057.86 | 1.244 |
| Third diffuser | 98.3 | 1057.86 | 115.9 | 1247.5 | 1.18 |
| Fourth diffuser | 141.3 | 1521.55 | 254.9 | 2743.6 | 1.8 |
| Fan section | 115.9 | 1247.5 | 141.3 | 1521.55 | 1.22 |
| Return duct between 4th diffuser and contraction | -- | -- | -- | -- | 1.033 |

## TEST EQUIPMENT

### Traverse Mechanism

Initially, feasibility studies were conducted, and subsequently a traverse mechanism was evolved that proved to be a simple serviceable design. This simple traverse mechanism essentially consisted of a pair of V-shaped pulleys, each situated at opposite sides of the tunnel wall. One pulley was driven by a small electric motor while the pulley on the opposite tunnel wall was idling. A thin cable was formed into an endless belt to ride under tension in the pulley grooves, and required tension was obtained by using a turnbuckle. The shafts of the pulleys were rotating in ball bearings housed in blocks which were joined to the walls by a bolt going through the channel, iron welded to the tunnel walls. This bolt allowed the block to be self-aligning. When the motor was driving the pulley, the cable moved across the tunnel. About 51 cm (20 in.) downstream from the moving cable and situated parallel with it, a single cable was stretched across the tunnel which remained stationary during the traverse operation. The set of cables - one moving, the other stationary - was capable of supporting as well as moving the sensor across the tunnel. The traverse setup is shown schematically in figure 2. A photograph of the moving components of the traverse mechanism near the wall of the tunnel is shown in figure 3(a).

### Sensor

The sensor employed was an anemometer consisting of a small propeller-driven generator housed inside a streamlined body frequently called a "bird" (ref. 1). A tail, extending from the rear of the body, aligned the bird with the flow direction when the wind was blowing [see fig. 3(a)]. The rotation of the propeller was found to be directly proportional to the flow velocity, which could be established accurately by using a frequency meter. A typical calibration graph of the

sensor is shown in figure 3(b). During traversing operations, location of the sensor across the tunnel was established by a potentionmeter geared to the shaft of the cable driving motor through a suitable reduction gear.

During the tests, the anemometer was positioned on top of a short vertical axle which was free to turn. The end of the axle was supported by a horizontal bar, one end of which was firmly fixed to the movable cable while the other end was fixed to a short tube through which passed the stationary support cable. Electric wires carrying the signals were let through a small opening in the tunnel wall, while the readout equipment was operating with the tunnel's computer system.

### Yawmeter

For the determination of flow angle and velocity downstream from the fan, a special yawmeter was installed behind the fan. It consisted of a tube 5.1 cm (2 in.) in diameter and 3.66-m (12-ft) long, extending vertically across the fan annulus as shown in figure 4. One end of the tube ended on the tunnel floor, the other at the nacelle. In this report this tube will be called the yaw tube. Seven sets of ports (measuring pressure) were distributed along the length of the yaw tube, each set consisting of a center and two side ports drilled at a central angle of 45° on each side of the center, as shown in figure 5. The 21 ports were connected to a sensitive pressure transducer by a pressure scanning device, and the pressures were recorded by the tunnel's computer-controlled data acquisition system.

## METHOD OF TESTING

The wind-tunnel circuit was originally planned to be surveyed at specific traverse locations marked on figure 1 from 1

to 19.* At each location a standard 15.2-cm (6-in.) channel iron, about 61-cm (24-in.) long, was welded to both sides at midheight of the tunnel. After the pulley blocks were placed into their respective positions, the cables were stretched to about 1112-N (250-lb) tension. Finally, the sensor was mounted and the potentiometer was set to zero position.

All surveys started with the sensor located near the inner wall of the tunnel, and it was activated to travel short distances. At each stop, while the sensor was stationary, the frequency of rotation was recorded several times to obtain a time average while the location of the sensor was read in millivolts. The traversing operation was repeated at each station for test section dynamic pressures of $q_r$ = 0.32, 0.58 and 1.00, respectively. It was noted that the sensor did not completely reach the wall and stopped at a distance that varied from 25 to 38 cm (10-15 in.) from the wall.

All velocity traverses with the bird were performed with the cables stretched across the tunnel only horizontally, while the flow pattern immediately downstream from the fan was established with the yaw tube in vertical position and at one location only.

## EXPERIMENTAL RESULTS

### Introduction

All velocity distributions presented in this report are normalized and $u/U_{max}$ is plotted against y/w, where $U_{max}$ = maximum axial velocity attained, y = distance from inner walls, and w = width of tunnel at the particular location under discussion. It is also noted that all traverses were only taken in the horizontal plane. Traverses were taken from

*Only the most important traverse stations were used in the tests.

T.S. 2 to T.S. 9 with the test section fully closed. Traverses were also made at a limited number of traverse stations with the test section fully open. Accordingly, the results are separately presented for the closed test section and for the open test section starting with T.S. 2 located near the exit from the test area. A tabulated guide to results is presented in table 2.

## Test Area Closed

First diffuser. - With the test area closed, the flow along the first diffuser showed the usual or "normal" development: namely, uniform velocity extending between boundary layers and a continuous boundary-layer growth with reasonable gradients near the walls. The thickness of the boundary layer at T.S. 2 was about 10 percent, as shown in figure 6(a); at T.S. 4 it was about 15 percent, as shown in figure 6(b); at T.S. 6 it was about 20 percent, as shown in figure 6(c) and at T.S. 8A it was about 25 percent, as shown in figure 6(d). One observed, however, that near the inner wall the boundary layer appeared thicker by about five percent than at the outer wall, and this observation held consistently all the way along the first diffuser, an indication that the flow at diffuser entry was not completely symmetrical.

In some tests the effect of changing the opening of the air breather (situated between T.S. 4 and 5) was manipulated, and the effect of the opening on the flow was studied. The results are shown in figures 7, 8, and 9. It appears that, in the immediate vicinity of the breather, the effects on the flow distribution were hardly noticeable, as shown in figures 7 and 8 where the extent of uniform flow is about the same with the breather closed, half open, or fully open.

The effect of the air breather at the exit section (T.S. 8A) is noticeable, however. When comparing figure 6(a) with figures 9(a) and 9(b), one finds the change in the width of the uniform flow slightly increasing and the gradients near the walls also

Table 2. Tabulated guide to results.

| Tunnel Component | Traverse Station (T.S.) | Figure Number | Air Breather |
|---|---|---|---|
| I. Velocity distribution with test section closed | | | |
| First Diffuser | 2 | 6(a) | Normal |
| | 4 | 6(b) | " |
| | 6 | 6(c) | " |
| | 8A | 6(d) | " |
| | 4 | 7 | Fully closed and open |
| | 5 | 8(a) | Closed |
| | 5 | 8(b) | ½ open |
| | 5 | 8(c) | Fully open |
| | 8A | 9(a) | ½ open |
| | 8A | 9(b) | Fully open |
| | 8A | 9(c) | Comparison |
| Second Diffuser | 9A | 10(a) | Normal |
| | 9B | 10(b) | |
| | 10A | 10(c) | |
| Third Diffuser | 11 | 11(a) | Normal |
| | 12 | 11(b) | |
| | 13 | 11(c) | |
| Fourth Diffuser | 14 | 12(a) | Normal |
| | 15 | 12(b) | |
| | 16 | 12(c) | |
| Contraction upstream | 17 | 13(a) | Normal |
| at inlet | 19 | 13(b) | |
| near exit | 20 | 14 | |
| II. Velocity distribution with test section open | | | |
| First Diffuser | 2 | 15(a) | |
| | 4 | 15(b) | |
| | 6 | 15(c) | |
| | 8A | 15(d) | |

Table 2. (Continued).

| Tunnel Component | Traverse Station (T.S.) | Figure Number | Air Breather |
|---|---|---|---|
| Second Diffuser | 10A | 15(e) | Normal |
| Third Diffuser | 12 | 15(f) | |
| | 13 | 15(g) | |
| Fourth Diffuser | -- | -- | |
| Contraction | | | |
| upstream | 17 | 15(h) | |
| at inlet | -- | -- | |
| near exit | 20 | 15(i) | |

III. Fan tests

| | |
|---|---|
| Total pressure rise | 16 |
| Axial velocity distribution | 17 |
| Yaw angle distribution | 18 |
| Pressure coefficient (around yaw tube) | 19 |
| Pressure differential | 20 |
| Velocity vector diagram | 21 |

improving. Figure 9(c) shows the curves from figures 6(a) and 9(b) superimposed for comparison - one representing the fully open air breather.

Flow through the first corner and second diffuser. - A traverse taken diagonally just downstream from the first corner turning vanes at T.S. 9A showed a definite change in the flow pattern from that at T.S. 8A. The velocity distribution [figure 10(a)] developed a defect in the vicinity of the center and the profile also shifted. This manifested itself in the high-velocity region's moving nearer to the inner wall while receding from the outer wall. Downstream from the flow control vanes at T.S. 9B, the defect became larger at low tunnel dynamic pressures ($q_r = 0.32$), and the velocity increased near the outer wall while decreasing near the inner wall. There appeared to be a rearrangement in the velocity distribution largely due to the presence of the flow control vanes, which allowed the flow to enter the second diffuser, with a more uniform flow.

Further downstream at T.S. 10A, the effect of the diffuser on the flow became marked [fig. 10(c)]. The dip in the vicinity of the center increased from 5 to about 7.5 percent, and a rapid boundary-layer buildup narrowed down the uniform velocity region to less than half of the tunnel width. The velocity distribution indeed looked like a slightly dented "sugarloaf."

Flow through the third diffuser. - At the inlet to the third diffuser (T.S. 11, downstream from the second corner) the profile flattened [fig. 11(a)] and thus improved to some extent due to the presence of the rather coarse screen* stretched across the corner vanes. However, the dip near the center had now increased to almost 10 percent, as shown in figure 11(a). In going downstream and towards the fan the velocity profile at T.S. 12 rapidly deteriorated at the outer wall, while at the inner wall the profile remained more or less unchanged, as shown in figure 11(b).

Just ahead of the fan at T.S. 13, however, the changes were quite dramatic. The flow became asymmetric about the centerline; and, while the profile near the inner wall could be considered acceptable, the outer wall profile became distorted and rather

*Screen mesh of 1.27 cm (2 per in.), 0.254 cm (.1 in.) wire diameter.

sensitive to viscous effects, as shown in figure 11(c). The large dip in the center region was now due to the presence of the fan hub. (The flow through the fan will be discussed in a later section of this report).

Flow in the fourth diffuser. - The flow in the fourth diffuser was found unsatisfactory, as shown in figure 12. Near the downstream end of the nacelle (T.S. 14) the velocity distribution was found asymmetric [fig. 12(a)] with two unequal velocity peaks. The larger peak ($u/U_{max} = 1$) was found nearer to the outer wall (at $y/w = 0.65$), while the smaller peak ($u/U_{max} = 0.85$) was found nearer to the inner wall (at $y/w = 0.4$). While a rather insignificant difference appeared in the near-wall regions ($y/w < 0.1$ or $> 0.9$), a significant difference between the velocity gradients appeared further inboard. Aroung $y/w = 0.2$, a zone of "hesitation" appeared where the gradient was practically zero. On the opposite side, around $y/w = 0.8$, the gradient was large. The center defect was naturally due to the presence of the nacelle. This velocity distribution may be considered critical in the development of the flow downstream.

Halfway along the fourth diffuser at T.S. 15, the flow appeared to be separated from the outer wall and the velocity peaked at a distance $y/w = 0.6$ for all speeds. The velocity distribution [fig. 12(b)] appeared to be sensitive to viscous (Reynolds number) effects and thus sensitive to tunnel q, resulting in a wide scatter of the observed values. The center velocity defect decreased with increasing distance from the nacelle, as may be anticipated, and the remaining defect was between 9 and 16 percent. The wide scatter was also probably due to an increased level of turbulence, which was visually noticeable when the sensor (bird) rotated periodically and changed direction erratically, thus indicating large and sudden changes in flow velocity and direction.

Finally, at exit from the fourth diffuser at T.S. 16, the flow [fig. 12(c)] appeared to be totally separated from the outer wall over 16 percent of the tunnel width. The velocity peaked at a

a distance of y/w = 0.33, in contrast to the distribution observed at T.S. 15. This indicated that a marked crossflow along the diffuser was also experienced. The defect near the center became noticeable at this station. Near the inner wall the flow appeared to be attached, while a velocity "level" was found between y/w = 0.07 and 0.18, a rather unusual occurrence in a flow.

Flow approaching the contraction and test section. - The flow between the third and fourth corner at T.S. 17 [fig. 13(a)] remained essentially of the same character as it was upstream from the third corner. It appeared to be fully separated from the outer wall, and the peak narrowed down to a ridge at a location of y/w ≈ 0.3 with the velocity rapidly falling off each side of the ridge. Thus the third corner had virtually no effect on the velocity distribution.

Downstream from the fourth corner at T.S. 19 [fig. 13(b)], flow improved to some extent after passing through the two sets of screens. The velocity peak slightly shifted outward but still remained too narrow to be considered an appropriate flow into a tunnel contraction. Scatter in the measurements was due to fluctuating flow and to the low velocities where the response of the sensor was least reliable. The velocity defect at y/w = 0.5 shown by the solid triangle symbol was found due to an oil slick on the screen - a warning to clean dirt periodically from screens!

Inside the contraction at T.S. 20, the flow distribution was found markedly different from the conditions prevailing upstream at entry to the contraction. It appears from figure 14 that the flow was much more uniform with two velocity peaks present, each in the vicinity of the walls. Between these peaks a "dished in" distribution was found, with a maximum defect of 4.5 percent at the center. It has been shown, based on previous measurements, that the flow distribution is uniform at inlet to the test section.

## Test Section Open

With the test area open the maximum tunnel speed was limited to $q_r = 0.58$ because of the large velocity fluctuations experienced. While marked changes in the distribution appeared along the first diffuser, only small changes were observed at other sections. Results of selected traverses taken around the tunnel circuit are shown in figure 15.

With the test section open, after the flow enters the first diffuser, at T.S.. 2, a boundary layer about 30 percent thick is experienced on each side, as shown in figure 15(a). Also, large velocity fluctuations were experienced near the wall, especially near the inner wall between y/w = 0.2 and 0.5. Further downstream, at T.S. 4, the boundary layer appeared to be 35 percent thick, and the velocity distribution showed considerable sensitivity to Reynolds number effects, as shown in figure 15(b). Some peculiarities could also be observed. For example, for tunnel $q_r = 0.20$, the flow distribution was more favorable than for $q_r = 0.32$, and the shapes of the curves also differed to some extent. Further downstream at T.S. 6, the curve representing the flow distribution for $q_r = 0.20$ had the shape of a bell, as shown in figure 15(c), while for $q_r = 0.32$ and 0.58 the curves in figure 15(b) show a "sugar-loaf" distribution. The difference near the walls between the curves in figure 15(b) is even more marked than in figure 15(a), further indicating high sensitivity to Reynolds number effects. Finally, at the end of the first diffuser, at T.S. 8A, the bell shape curve previously observed at T.S. 6 for $q_r = 0.20$ changed and developed a dip near the center, while the "sugar-loaf" for $q_r = 0.32$ and 0.58 appeared almost parabolic, as shown in figure 15(d). In summary, as far as the first diffuser was concerned, with the test section open, the flow at $q_r = 0.20$ "filled" the diffuser more readily than that at other dynamic pressures.

Downstream from the first corner at T.S. 10A, the flow pattern again assumed about the same distribution as upstream at T.S. 8A as shown in figure 15(e). For tunnel $q_r = 0.20$, the defect ramained about the same as upstream while the "sugar-loaf"

pattern changed to a parabolic shape for $q_r$ = 0.32 and 0.58, suggesting the presence of a thicker boundary layer for a higher q. This was a surprising result which could not be readily explained from the theory of boundary layers. There must have been some interference from the open test section that influenced the inflow to the first diffuser at higher tunnel speeds, which, incidentally, needs further study.

Downstream from the second corner, the flow was found erratic at T.S. 12. A large defect appeared in the center at $q_r$ = 0.20 and a somewhat smaller defect appeared for $q_r$ = 0.32 and 0.58, as shown in figure 15(f). This defect was also found when the test section was closed due to the presence of the fan. At the conclusion of these tests, it was found that the tunnel q was probably too low for the flow sensor. However, just upstream from the fan at T.S. 13, the flow distribution as shown in figure 15(g) was found almost identical with the distribution when the test section was closed [see figure 12(c) for comparison].

Between the third and fourth corner, the open test section did not appreciably affect the flow, which peaked at a distance y/w = 0.4 from the inner wall and fully separated at the outer wall as shown in figure 15(h). When comparing figure 14(a) with figure 15(h), one finds the latter has a more rounded peak and the former a sharper peak. However, the difference is small and may be due to an experimental error.

The flow pattern inside the contraction at T.S. 20 was remarkably similar to that obtained with the closed test area as shown in figure 15(i).

## Comparison Between Closed and Open Test Section

When comparing results between the closed and open test section, one finds that in the first diffuser (adjoining the test section) the flow markedly changed characteristics. While with the test section closed the blockage at the diffuser entry was small, with the test area open the blockage was considerably larger. In other words, with the test section closed, the velocity

distribution at inlet was uniform almost all the way across the stream (except for a small region near the wall), while with the test section open the uniform portion of the distribution was much narrower. It would be interesting to take a vertical traverse at this traverse station (T.S. 2).

In following the flow along the first diffuser, by the time the exit was reached (T.S. 8A), the velocity distribution was almost parabolic in shape for the higher tunnel $q$ with no uniform portion present. Upstream from the fan (T.S. 12) the flow distribution results were found to be unsatisfactory. Scatter of the experimental data could be attributed to large velocity fluctuations in the flow, leading to some erratic results. The influence of the test section (being open or closed) was totally absent in the flow sections located between the third and fourth corner and also inside the contraction (T.S. 17 and 20).

## FAN PERFORMANCE RESULTS

The tests were performed at 3 fan speeds: 143, 192, and 253 rpm, corresponding to tunnel $q_r$ = 0.32, 0.58, and 1.00. Prior to testing the yaw tube was aligned with the tunnel axis using a simple sighting technique that employed a transit-telescope. At zero yaw angle the central tube faced the airstream. Prior to testing, the tube was rotated to a preset yaw angle $\delta$ and each test run (during which all pressures were recorded) was repeated in turn for angles of 25°, 35°, and 45°,respectively, while the speed of the fan was kept constant. This was necessary because the limit of linearity of the yaw tube calibration was ± 10° (see Appendix A), and the flow angles downstream from the fan varied between 25° and 45°.

Test results were evaluated from the measured values of pressure differentials. For the determination of yaw, the differential $p_1 - p_3$ was employed, while $p_2 - \frac{1}{2}(p_1 + p_3)$ was used to determine $q$.

The total pressure rise across the fan is shown in figure 16. In going form the hub towards the tip, a gradual fall in total pressure rise was experienced. This is undesirable because it causes vorticity to be shed into the flow. However, the fall was not very large in comparison to the sudden rise near the tip, which points to stall, or at least near stall, conditions. In reality the rise may not be as large as shown owing to the decrease in lift-drag ratio when the blade tip was operating near stall conditions. This decrease has not been taken into consideration when calculating the pressure rise. (See Appendix B.)

In figure 17, the axial velocity distribution $V_a$ is plotted against normalized radial distance r/R for three tunnel q-s, where the axial velocity was calculated from the relation $V_a = V_o \cos \phi$). It appears from figure 17 that the axial velocity varied across the fan annulus. While the variation was relatively small between r/R = 0.5 and 0.9, near the hub (0.4 to 0.5) and near the tip (0.9 to 1) the variation was rather large. Near the tip the fall-off in $V_a$ signifies the near-stall conditions owing to large buildup in the boundary layer ahead of the fan, while "run-ahead" conditions existing near the hub signify the effects of the fairing around which large accelerations take place. The assumed velocity distribution at a test section $q_r = 1.0$ upon which the fan design is based is shown as a dashed line in figure 17 and it agrees remarkably well with the experimentally obtained values between r/R = 0.8 and 0.9. However, discrepancies between assumption and results appear at other radial locations. The experimental data curves seem to have about the same shape for all three speeds.

The yaw angles measured at high fan speed (253 rpm) are shown in figure 18, which shows the range of yaw angles lying roughly between 25° and 40° except near the tip, where the sudden rise due to tip stall was experienced. The fall-off in $V_a$ is also due to the increase in $\phi$ at the tip. Low axial velocity resulted in a low advance ratio, which in turn led to low blade element efficiency. In addition, low axial velocity also caused high lift at the tip, which brought the tip region to near-stall condition

and also caused high drag. These effects resulted in increased blockage of inflow to the fourth diffuser and made it unable to perform satisfactorily.

## DISCUSSION

It appears from the experimental results that the flow deteriorates as it moves around the tunnel circuit. Starting the analysis of the results from the inlet to the first diffuser (T.S. 2), one finds a satisfactory velocity distribution that closely follows the familiar, full developed, turbulent "flow-in-pipe" parabolic pattern. Therefore, one can anticipate that at exit from the first diffuser (T.S. 8A) the flow will be acceptable in so far as a thick boundary-layer growth observed on both sides is considered a normal feature of diffusers. All the way along the first diffuser the maximum velocity, extending between boundary layers, remained constant across the rest of the cross section. The small defect near the center was probably caused by the turning vanes, and may therefore be ignored.

The problems started downstream from the first corner at T.S. 9A where the velocity distribution near the outer wall showed a marked difference as compared with the inner wall, inasmuch as the velocity fell below that experienced near the inner wall. The first reason for this is probably due to streamline curvature. Since the radius of the streamlines must become larger in turning near the outer wall, the flow cannot fully extend to the wall without an appreciable decrease in the velocity gradient. The second reason is due to the thick boundary layers upstream from the corner, which decreased the flow near the walls and thus made turning in and outboard less effective. Generally, design data for turning vanes assume "wall-to-wall" uniform flow upstream, which, being an ideal assumption, may not be readily applied in wind tunnels of the closed-circuit design.

Additional diffusion in the second diffuser further increased the boundary-layer thickness, thus making the profile more peaked as shown at T.S. 10A, where a more marked velocity defect also

became noticeable. At entry to the third diffuser, at T.S. 11, some improvement in the profile could be observed which was due to the presence of a coarse screen applied across the second corner. However, while the defect became narrower, at the same time it increased its depth. The flow markedly deteriorated between T.S. 11 and T.S. 12. Indeed, at T.S. 12 the outer velocity profile already began to show some signs of an imminent separation. at T.S. 13 the defect widened and deepened because the presence of the fan hub was propagated by the flow upstream. Therefore, it may be assumed that the defects found further upstream could also have been caused by the fan hub. While a large "dip" between two velocity peaks immediately ahead of the fan could be expected from flow through the annulus around the nacelle, it was disturbing that the velocity gradients near the opposite walls appeared unequal. This added to the complexity of flow through the fan, because normally one expects an axial flow fan to operate with an axially symmetrical velocity distribution approaching the fan annulus. The flow's being unsymmetrical suggests that the rotating fan blades must experience different angles of attack on opposite sides, thus producing different lift and different pressure rise. As a result, the flow downstream must also become different on opposite sides, as shown at T.S. 14, where velocity peaked at about $y/w = 0.65$, which was consistent with the lower axial velocity in this region shown at T.S. 13.

In the fourth diffuser the flow distribution at T.S. 15 and T. S. 16 clearly indicated stalled regions on the outer wall. Within 16 percent of the outer region the velocity fell to zero intermittently. Inside this stalled region it was observed that the sensor (bird) behaved erratically. Periodically it stopped and started rotation, and once in a while it also abruptly changed direction, thus indicating intermittent flow known as "transitory stall."

A remarkable change in flow direction was also experienced in the fourth diffuser. In going from T.S. 15 to 16, the peak velocity shifted from the outer wall towards the inner wall, changing position from $y/w = 0.6$ to 0.34. This clearly indicated a crossflow that may have been caused by the flow approaching the third corner.

The effects of the third and fourth corners on the flow and the equalizing effects of the screens upstream from the contraction only helped to round the velocity profile to a minor extent. The profile remained excessively peaked as shown graphically at T.S. 19, and thus must be considered unsatisfactory even if the flow at exit from the contraction was found to be uniform.

## CONCLUSIONS AND RECOMMENDATIONS

An investigation into the flow characteristics of the V/STOL tunnel located at NASA/LaRC has been conducted. The results of the investigations show an interaction between tunnel components, each component adversely affecting other components downstream and, to some extent, upstream. The components which appeared to have the largest influence on the flow were the corners. This in turn caused other components, like the diffusers and the fan, to perform unsatisfactorily. The following recommendations are made:

1. The flow downstream from the first diffuser needs to be corrected so that the flow into the second corner becomes more uniform. The same suggestion applies to the second corner.

2. The flow approaching the fan needs improving.

3. The flow patterns inside the large diffuser following the fan are a matter of considerable concern. The transitory stall on the outer side needs to be eliminated by correcting the flow distribution at entry to the diffuser.

4. Flow into the contraction was found to have been nonuniform, and the installation of additional screens may become necessary if the flow upstream cannot be satisfactorily corrected.

5. Effects of the open test section on the flow into the first diffuser need to be further studied, and the large fluctuations experienced in the test section need to be controlled.

## APPENDIX A

## CALIBRATION CURVES FOR THE YAW TUBE

The calibration curves obtained on the yaw tube setup in the wind tunnel were compared with results of pressure distribution around a circular cylinder (ref. 2). Even though small variations in port location were observed among the seven sets of pressure ports, the calibration results compare favorably with the results obtained when using the pressure distribution data for a circular cylinder at an appropriate Reynolds number. Hence for the fan performance measurements a calibration based on pressure distribution data was employed.

Introducing the nondimensional pressure coefficient $C_p = p/q$, one obtains from the distribution curve shown in figure 19, where $C_p$ is plotted against $\theta$, the difference between static ports 1 and 3

$$\frac{\Delta p}{q} = \frac{p_1 - p_3}{q} = C_{p_1} - C_{p_3} \tag{A1}$$

The values of $C_{p_1}$ and $C_{p_3}$ are obtained by simply taking for angle $\theta_1$ the angle $\theta + 45$ and for angle $\theta_3$ the angle $45 - \theta$. (Note $\theta_2 = \theta$ and that here $q = 1/2\rho U_\infty^2$, where $U_\infty$ is the approach velocity far upstream).

By defining $Q_p = p_2 - 1/2(p_1 + p_3)$ one obtains

$$\frac{Q_p}{q} = C_{p_2} - 1/2(C_{p_1} + C_{p_3})$$

$$\text{hence} \quad \frac{\Delta p}{Q_p} = \left(\frac{\Delta p}{q}\right)\left(\frac{q}{Q_p}\right) = \frac{C_{p_1} - C_{p_3}}{C_{p_2} - 1/2(C_{p_1} + C_{p_3})} \tag{A2}$$

In figure 20 both $\frac{\Delta p}{q}$ and $\frac{\Delta p}{Q_p}$ are plotted against yaw angle $\theta$. It appears that both curves are linear between $\pm 10°$, and inside this linear region one finds that

$$\frac{\Delta p}{q} \simeq \frac{\theta}{10.333} \tag{A3}$$

and

$$\frac{\Delta p}{Q_p} \simeq \frac{\theta}{14.333} \tag{A4}$$

From the experimentally obtained values of $\Delta p$ and $Q_p$, the dynamic head $q$, and hence the flow velocity and its direction can be calculated. Substitution of $\Delta p$ from equation (A3) into equation (A4) leads to $Q_p/q = 14.333/10.333 = 1.387$. With $\rho = 0.00227$ one obtains from the relation $q = 1/2\rho V_o^2$*

$$V_o = 25.2\sqrt{Q_p} \tag{A5}$$

The yaw angle can be determined by solving equation (A4) for $\theta$

$$\theta = 14.333 \frac{\Delta p}{Q_p} \tag{A6}$$

Finally, if the yaw tube is positioned with a preset angle $\delta$ enclosed with the tunnel centerline, one obtains the yaw angle

$$\phi = \delta + \theta \tag{A7}$$

*Note, that $V_o$ is the approach velocity to the yaw tube and is the absolute velocity downstream from the fan blades.

## APPENDIX B

## NOTES ON FAN PERFORMANCE

### Introduction

In commercial practice, a fan's performance is generally judged by the overall pressure rise and efficiency it produces. These values can be simply obtained from weighted average measurements for which the methods are specified in standard fan codes (ref. 3). In the case of axial flow fans, average measurements of performance have limited usefulness; they generally suffer from lack of information on the radial distribution of such variables as the local values of pressure rise, of blade element efficiency, of through-flow velocity, etc., which can indeed vary a great deal along the blade. Detailed distribution measurements of the relevant variables facilitate analysis of performance, and the information obtained may be employed to locate areas of unsatisfactory performance. Ultimately, the weighted average values can be calculated by simple summation methods.

Requirements for high efficiency demand that all blades be operated at or near the maximum lift-drag ratio of the particular airfoil profile employed in the design with the flow maintaining a suitable advance ratio J. The desirable range for J falls between 0.2 and 1.0; below 0.2 the efficiency falls off rapidly with decreasing J (ref. 4).

In order to analyze a given axial flow fan's performance, it is necessary to first measure at various radial locations the magnitude ($V_o$) and direction ($\phi$) of the absolute velocity leaving the fan blade. Resolving $V_o$ into tangential and azial direction, one obtains the components $V_w$ and $V_a$, respectively, and with these components the velocity vector diagrams can be established for both the leading and the trailing edge (ref. 4). By vectorially adding $V_a$ to the blade speed $V_t$, one obtains the relative velocity $U_1$ at the leading edge, while $U_2$ at the trailing edge is obtained by adding $V_o$ to $V_t$ as shown in figures 21(a) and 21(b). Upon superimposing figures 21(a) and 21(b), one obtains figure 21(c), where the mean of $U_1$ and $U_2$ is shown as $U_m$

(drawn by a dashed line) which intersects the plane of rotation t with an angle of $\beta_m$. At a radial location r, the blade profile inclines with the angle $\gamma$ to the plane of rotation; thus the mean blade incidence angle $\alpha_m$ becomes the difference $\gamma - \beta_m$.

The procedure followed in the present analysis was to first assume a reasonable fixed value for the lift-drag ratio needed for the calculation of the blade element efficiency. The local total pressure rise across the fan was calculated from the relationship

$$\Delta p_t = \rho V_t V_w \eta_b$$

## Calculation of Pressure Rise Across the Fan

The theoretical pressure rise in fans is given by the well-known formula for Euler lift (ref. 5):

$$H_E = \frac{V_t V_w}{g}$$

where $V_t = \omega r$ is the tangential speed of the rotating blade at radius r and $V_w$ is the whirl velocity of the stream leaving the blade (assuming zero whirl at blade leading edge). Since $H_E g = \Delta p_E/\rho$ we may write

$$\Delta p_E = \rho V_t V_w$$

Due to viscous effects the actual pressure rise is somewhat less and this is accounted for by introducing the blade element efficiency $\eta_b$. Thus

$$\Delta p_t = \rho V_t V_w \eta_b \qquad \text{(B1)}$$

Further, by introducing $\sigma = r/R$ the tangential speed becomes

$$V_t = \frac{\pi n}{30}\left(\frac{r}{R}\right) R$$

Since the radius of the fan at tip R = 6.1 m (20 ft), one obtains

$$V_t = \frac{2}{3}\pi n\sigma \tag{B2}$$

Since the whirl velocity

$$V_w = V_o \sin \phi \tag{B3}$$

substitution for $V_o$ from equation (A5) leads to

$$V_w = 25.2\sqrt{Q_p} \sin \phi \tag{B4}$$

Substituting equations (B2) and (B4) into equation (B1) yields the pressure rise

$$\Delta p_t = \rho(\frac{2}{3}\pi n\sigma)(25.2\ Q_p \sin \phi)\eta_b$$

During the tests the density was found to be $\rho = 0.00227$ lb/ft$^3$ and with the conversion factor 1 inch W.G. = 5.2 lb/ft, one obtains

$$\Delta p_t = 0.023 n\sigma\sqrt{Q_p} \sin \phi\ \eta_b \text{ (inches of W.G.)} \tag{B5}$$

In order to complete the calculation it is necessary to estimate the value of the blade efficiency.

For relatively low whirl velocities experienced in axial flow fans the blade element efficiency

$$\eta_b \simeq \frac{J(K-J)}{I + J\ K} \tag{B6}$$

where $K = C_L/C_D$ and $J = V_a/V_t$. Since the axial velocity

$$V_a = V \cos \phi \tag{B7}$$

substition for $V$ from equation (A5) leads to

$$V_a = 25.2\sqrt{Q_p} \cos \phi \tag{B8}$$

Upon dividing equation (B9) by equation (B2), one obtains for the advance ratio

$$J = 12.03 \frac{\sqrt{Q_p} \cos \phi}{\sigma} \qquad \text{(B9)}$$

For the calculation of $\eta_b$ the value of $K$ was assumed to be 25.

## REFERENCES


1. Kershner, D.D.: Miniature Flow-Direction and Airspeed Sensor for Airplanes. NASA Technical Paper 1467, 1979.

2. Fage, A.; and Faulkner, V.M.: Further Experiments on the Flow Around a Cylinder. ARC, R & M 1369, 1931.

2. Flow Metering. British Standard Code 1042, 1942.

4. Patterson, G.N.: Ducted Fans: Design for High Efficiency. Australian Council Aero. Rep. ACA, 1944.

5. Barna, P.S.: Fluid Mechanics for Engineers. 3rd. Edition, Butterworth, 1969.

FIGURES

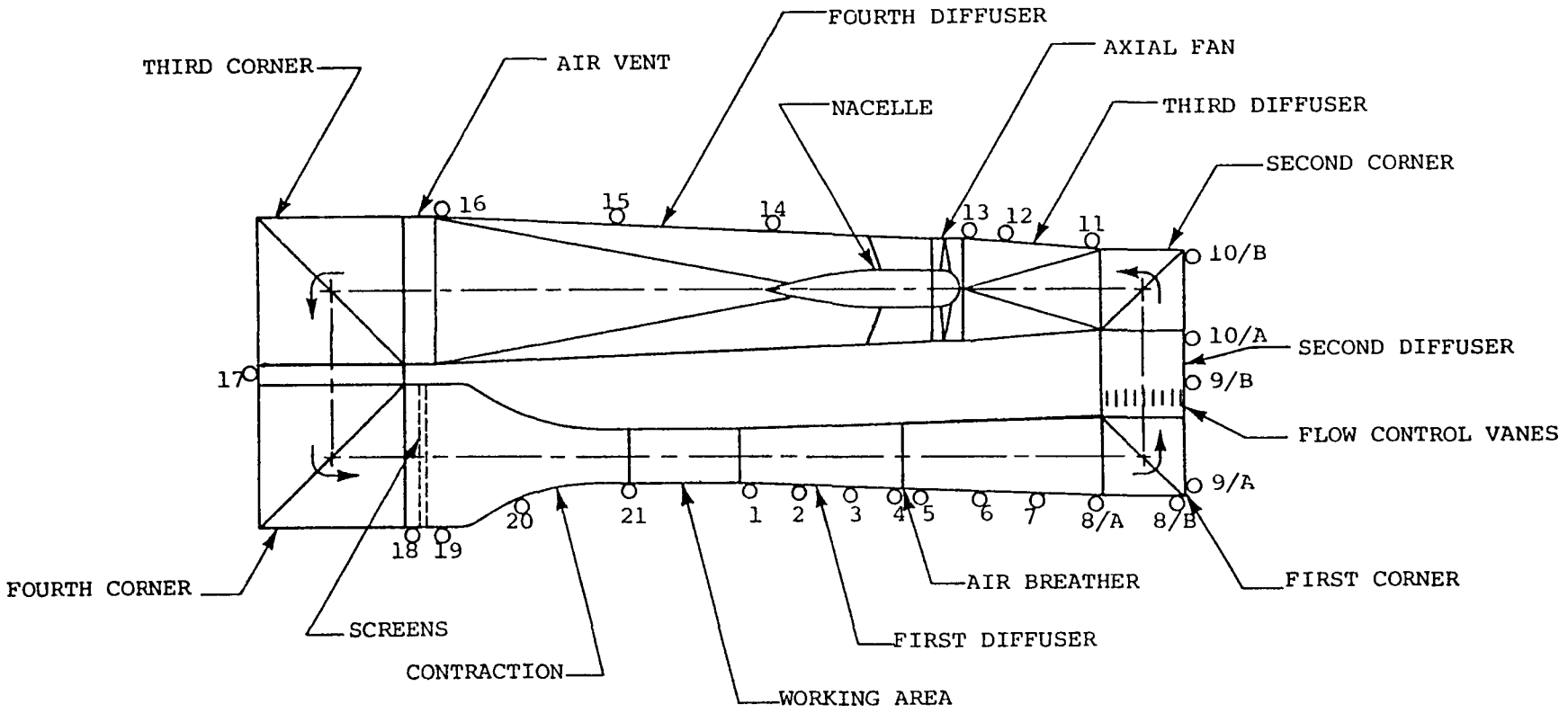


Figure 1. Plan view of the V/STOL tunnel.

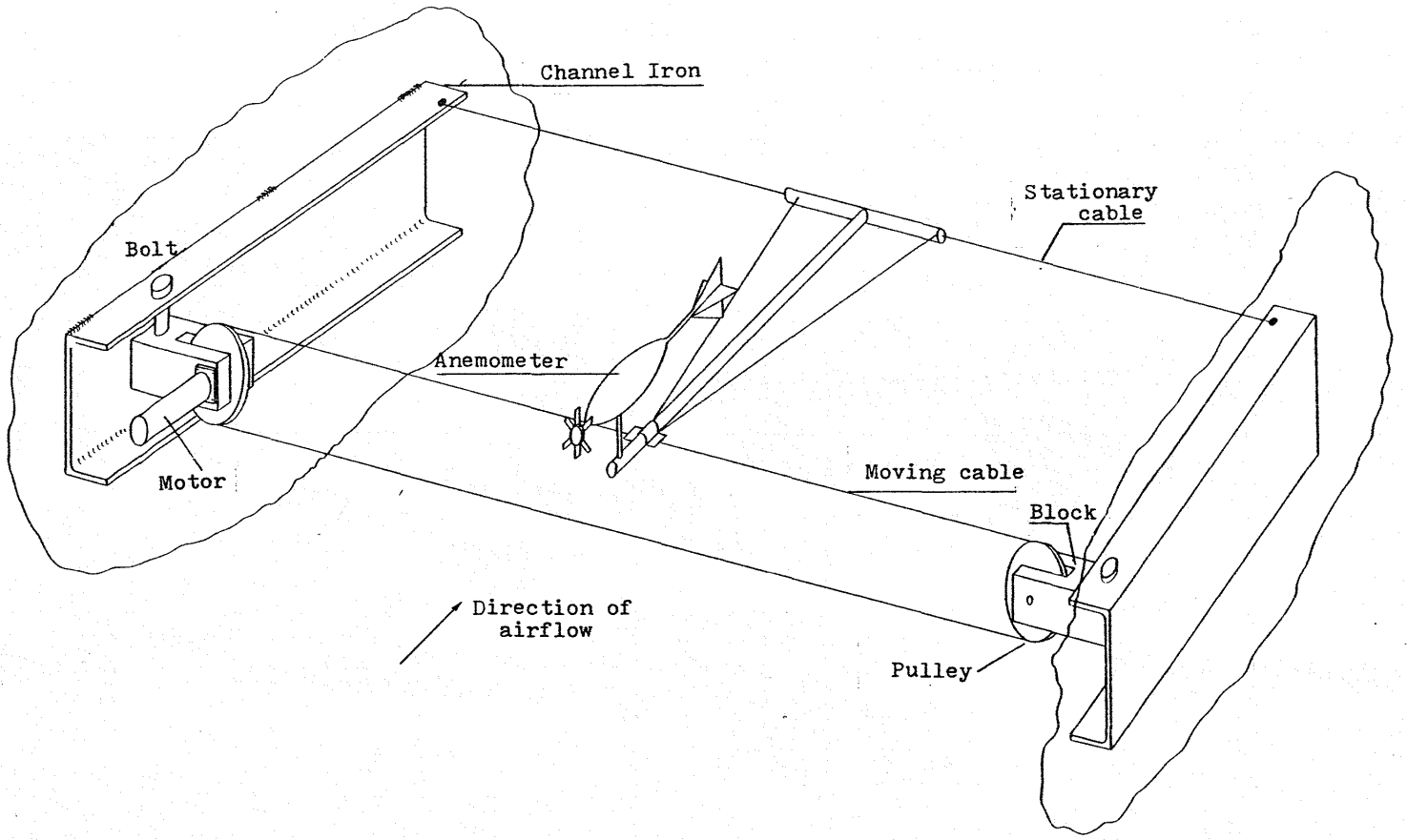


Figure 2. Tunnel traverse mechanism.

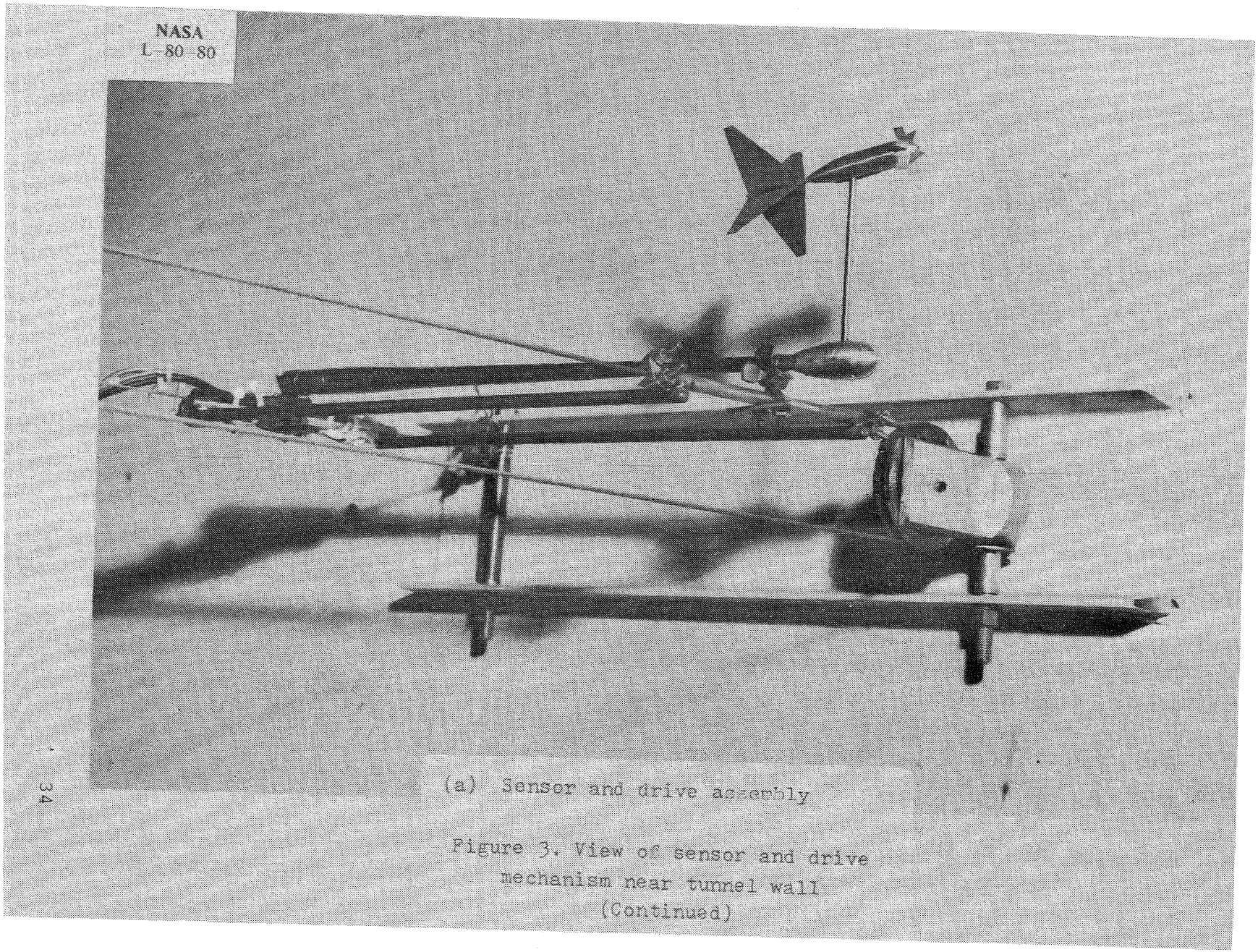


(a) Sensor and drive assembly

Figure 3. View of sensor and drive mechanism near tunnel wall (Continued)

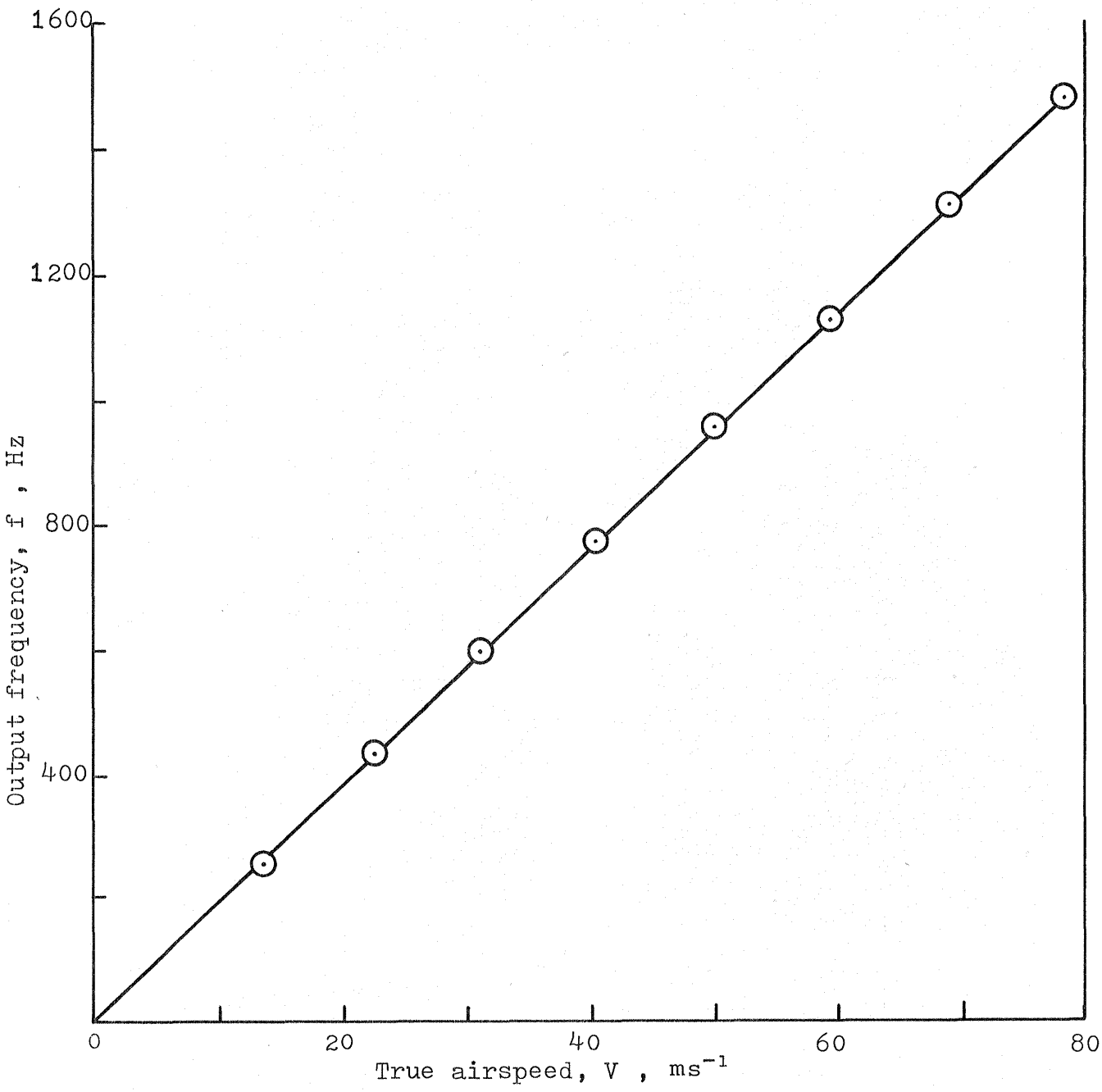


(b) Sensor calibration graph

Figure 3 Concluded

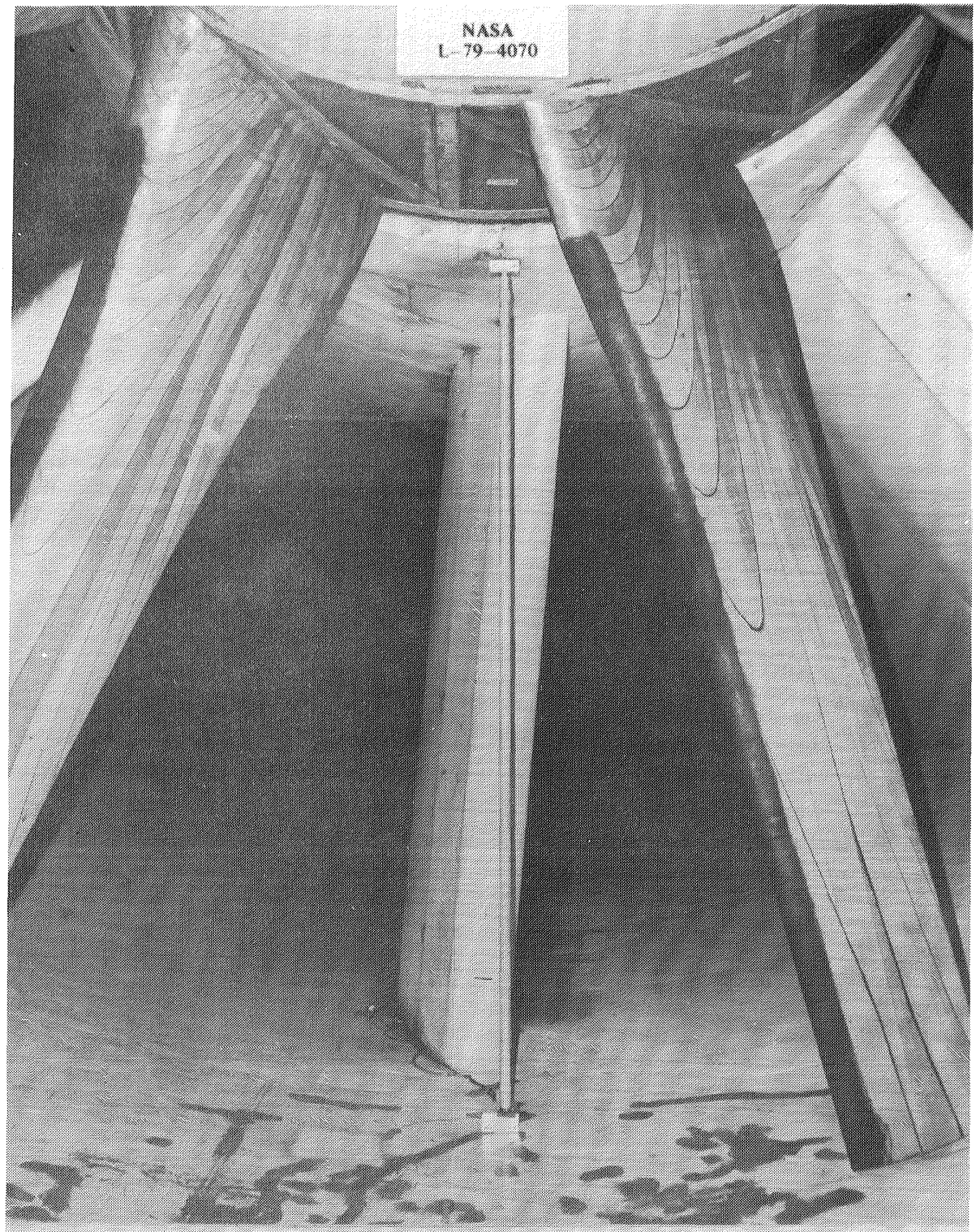


Figure 4. Yaw tube installed behind fan.

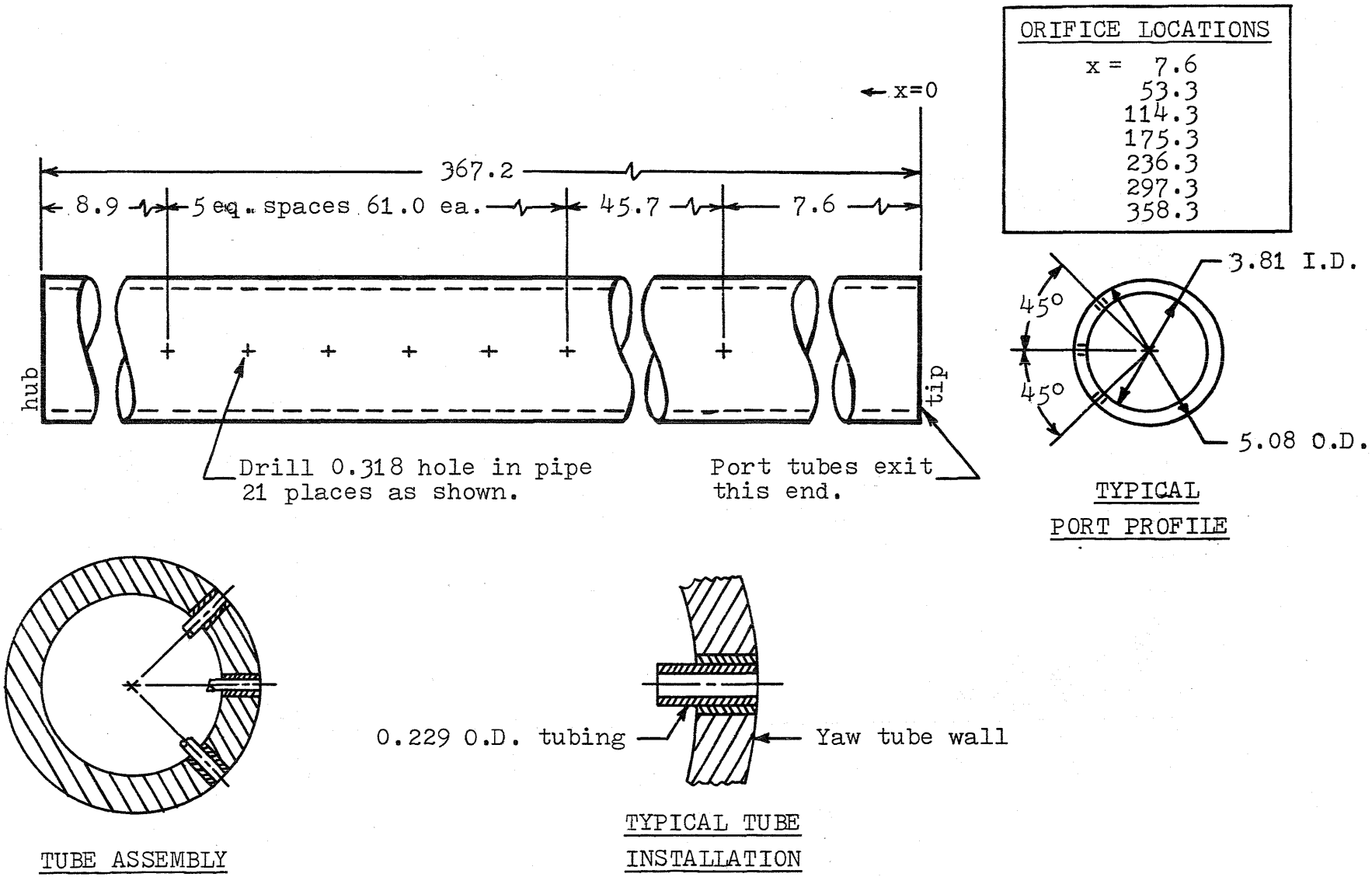


Figure 5. Details of yaw tube.
(All dimensions in
centimeters.)

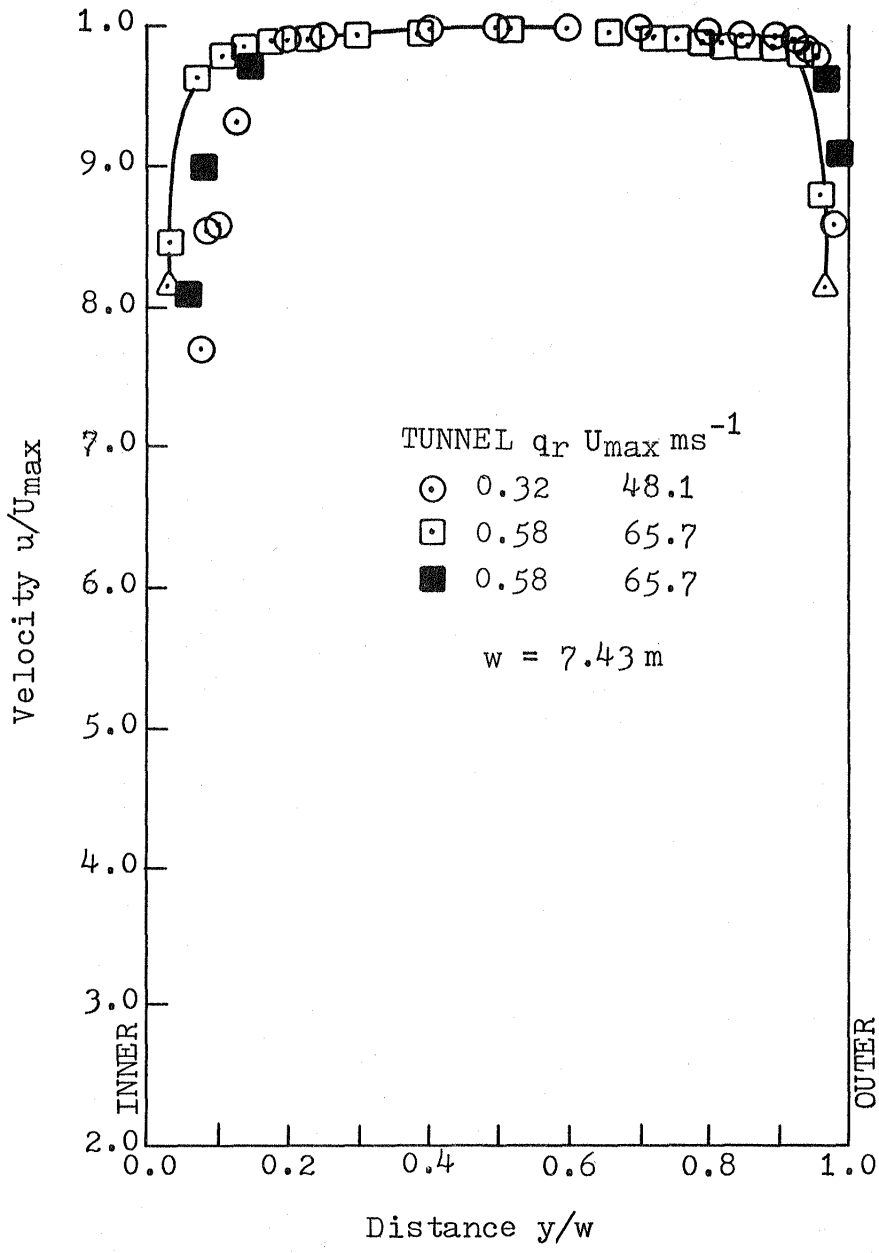


(a) Traverse Station 2

Figure 6. Velocity distribution in the first diffuser.

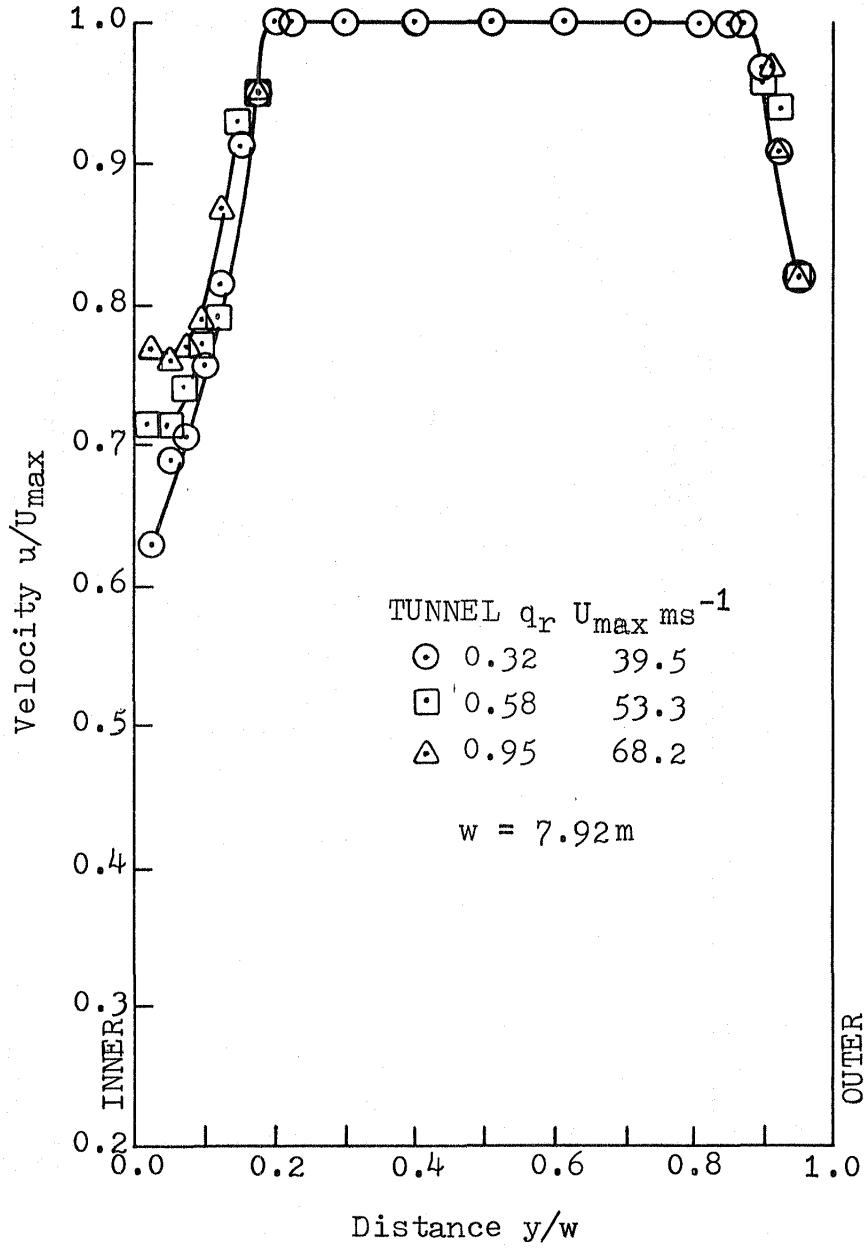


(b) Traverse Station 4

Figure 6 Continued

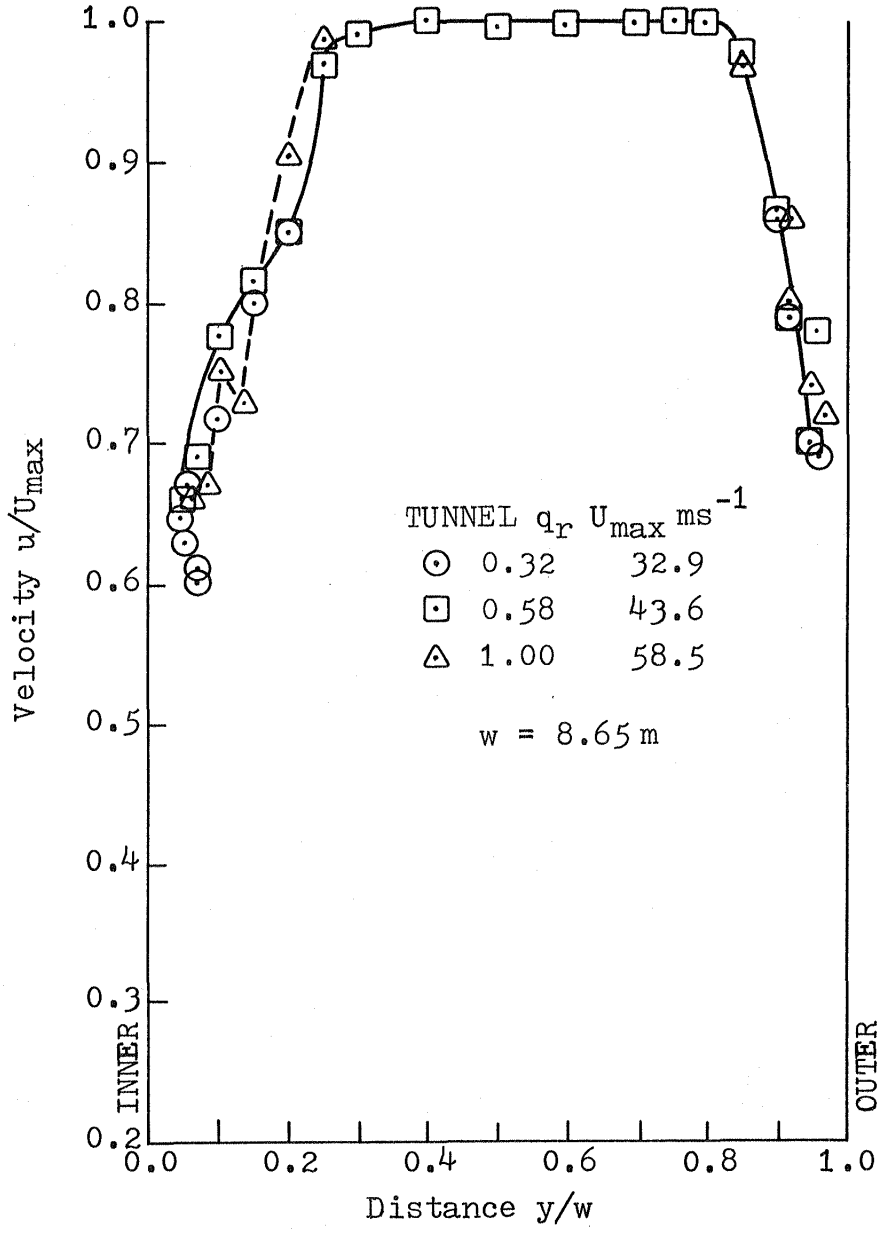


(c) Traverse Station 6

Figure 6 Continued

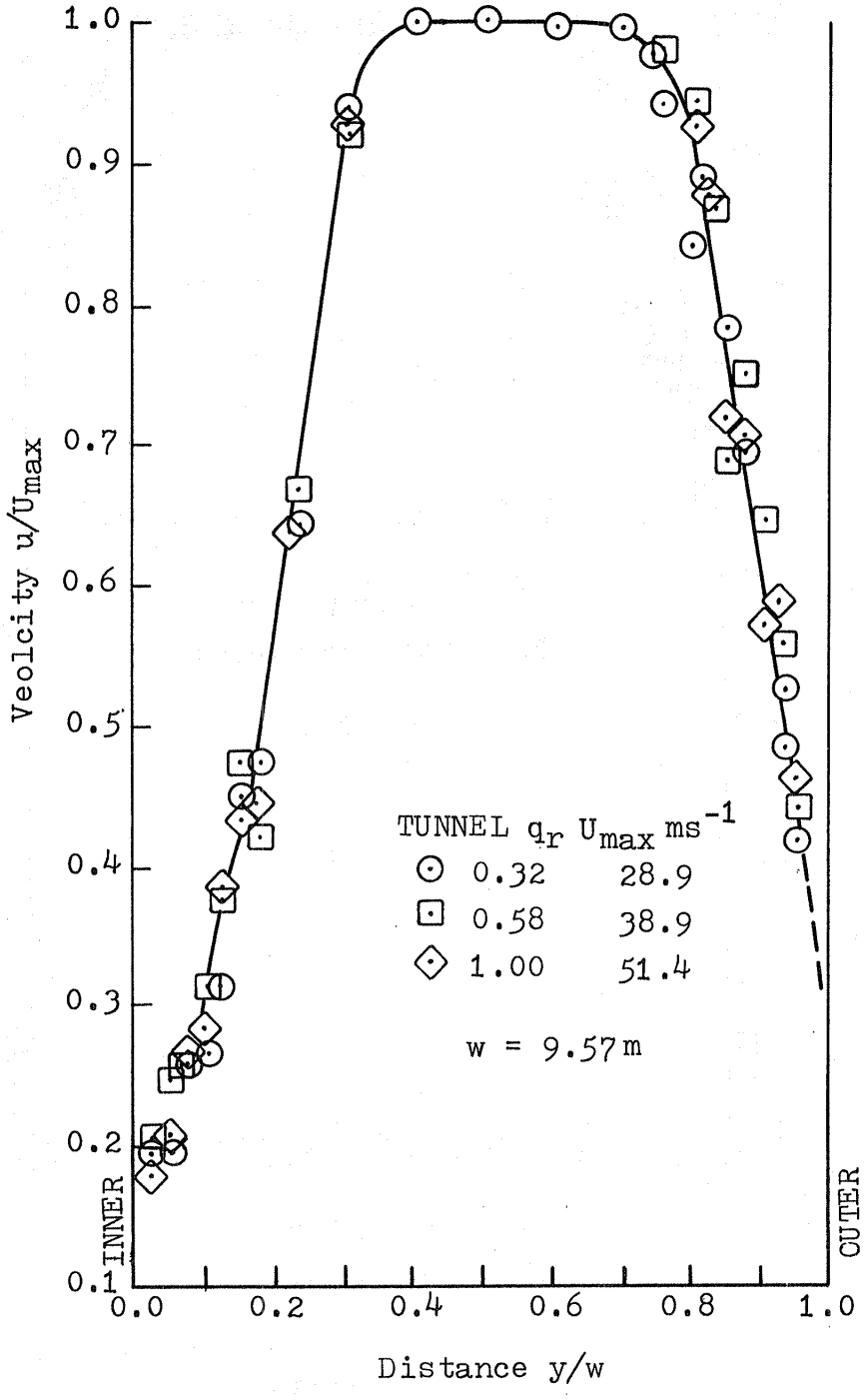


(d) Traverse Station 8A

Figure 6 Concluded

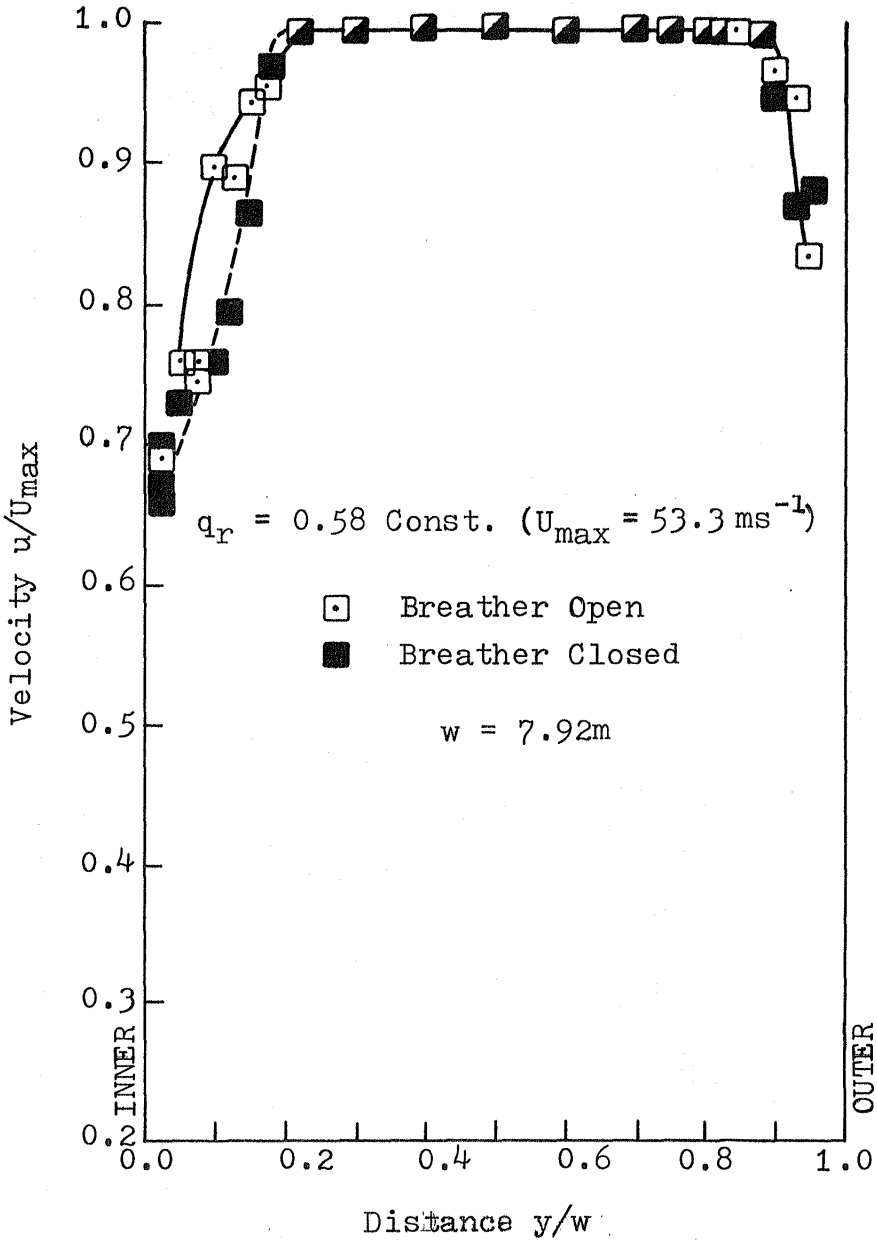


Figure 7. Effects of air breather on flow upstream (T.S.4) in first diffuser.

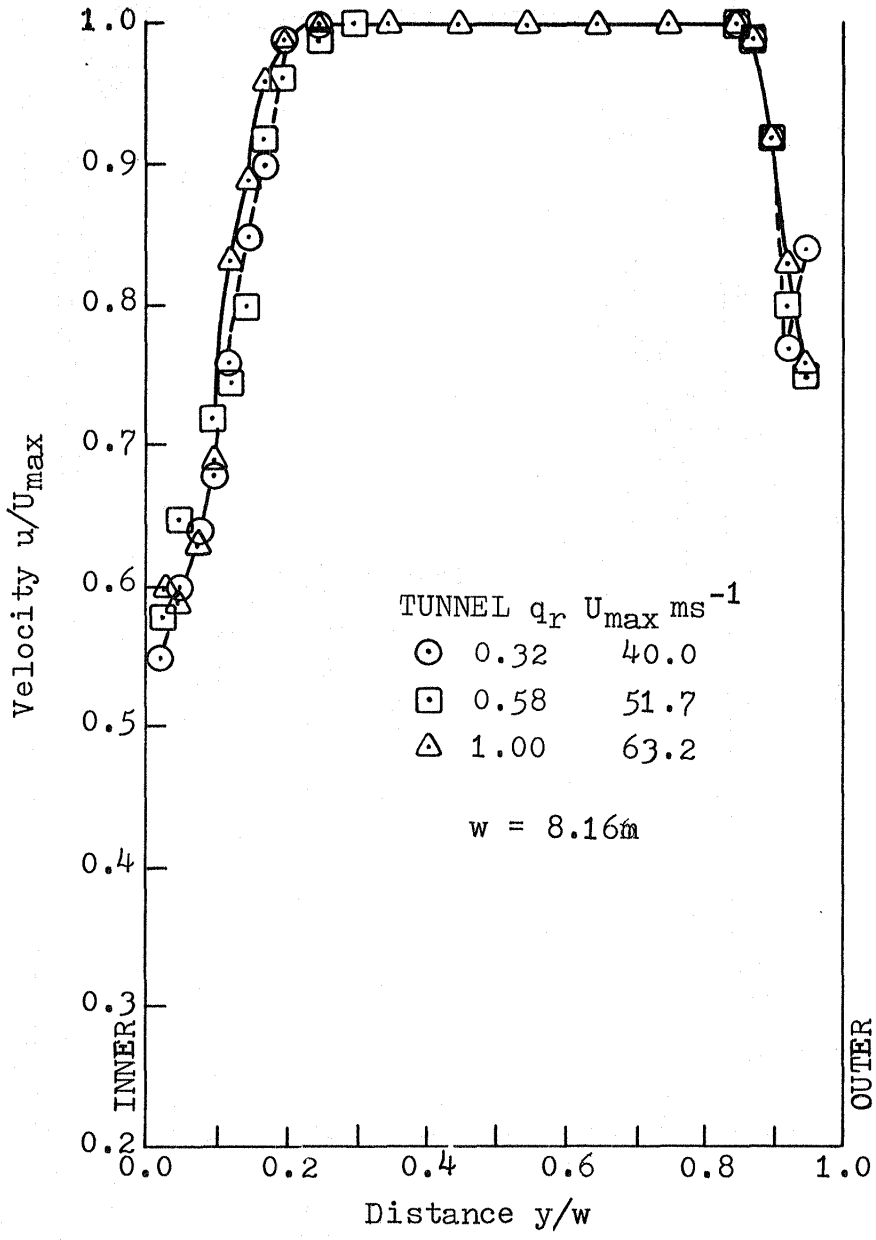


(a) Air breather fully closed

Figure 8. Effects of air breather on flow downstream in first diffuser (T.S.5).

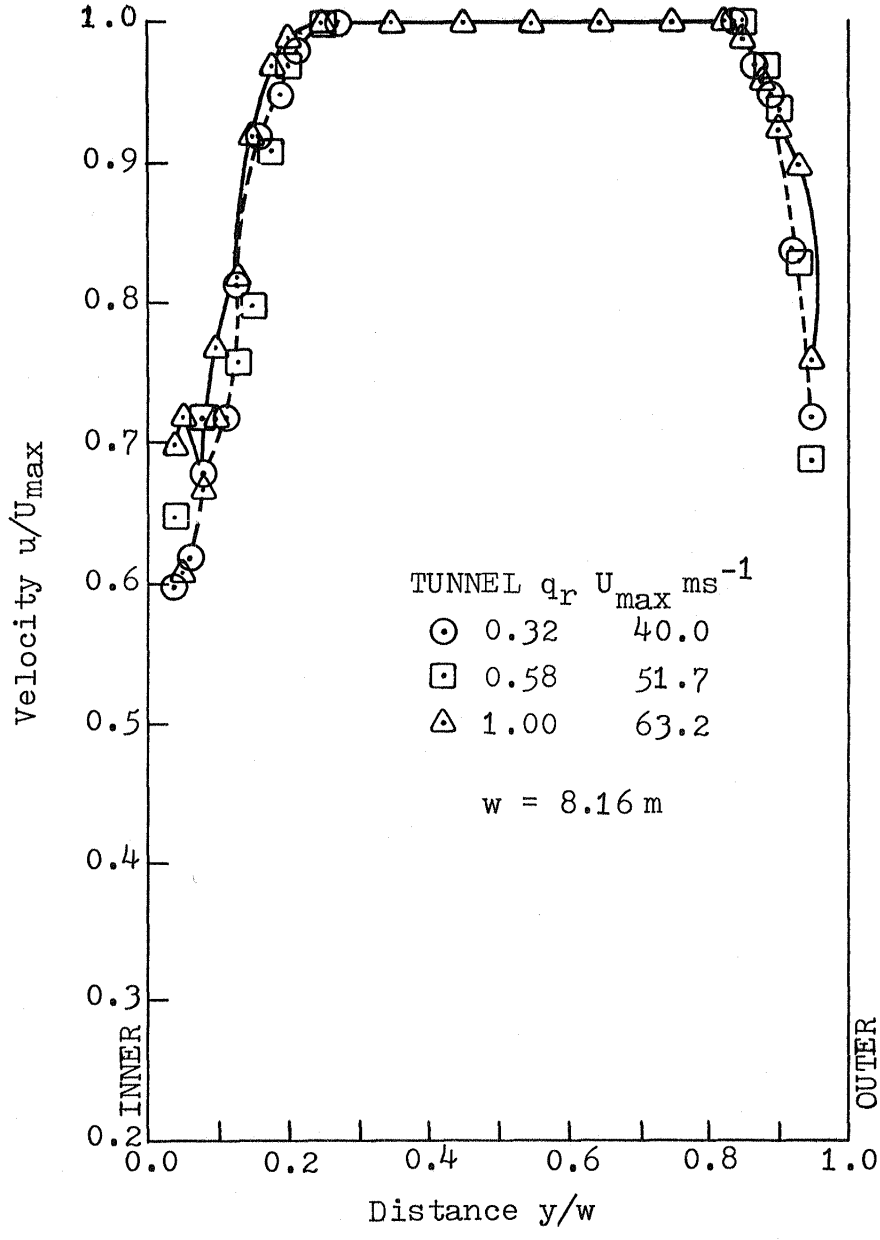


(b) Air breather half open (6 in.)

Figure 8 Continued

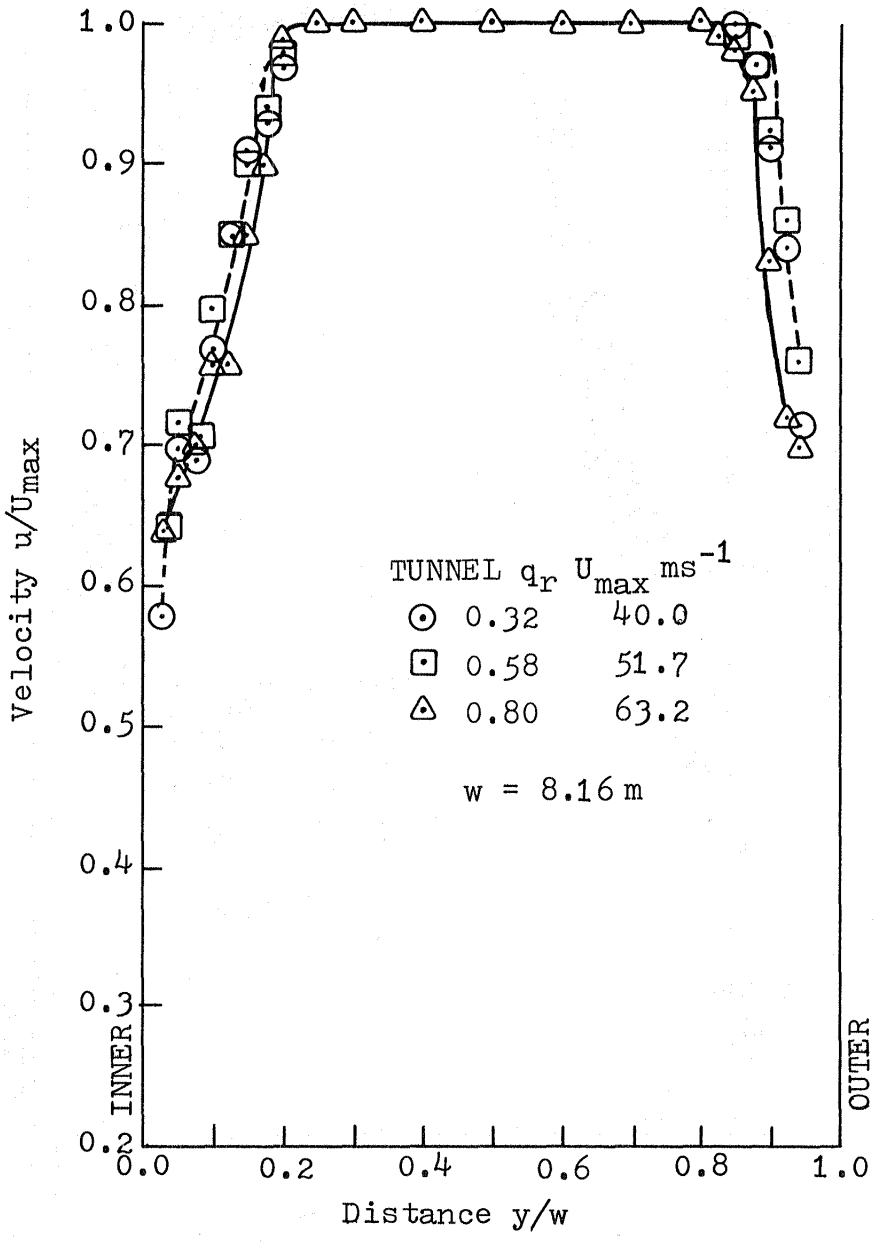


(c) Air breather fully open

Figure 8 Concluded

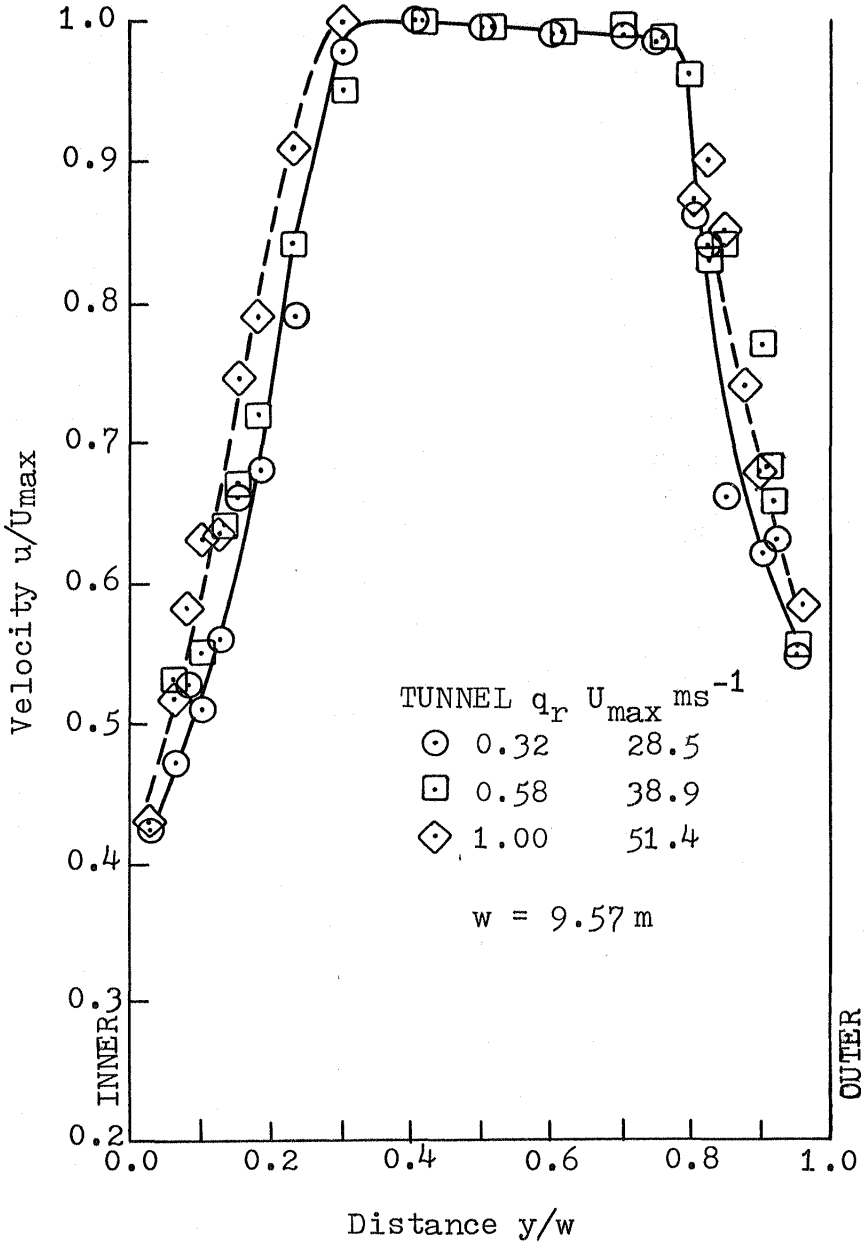


(a) Air breather half open

Figure 9. Effects of the air breather on the flow at exit from the first diffuser (T.S. 8A)

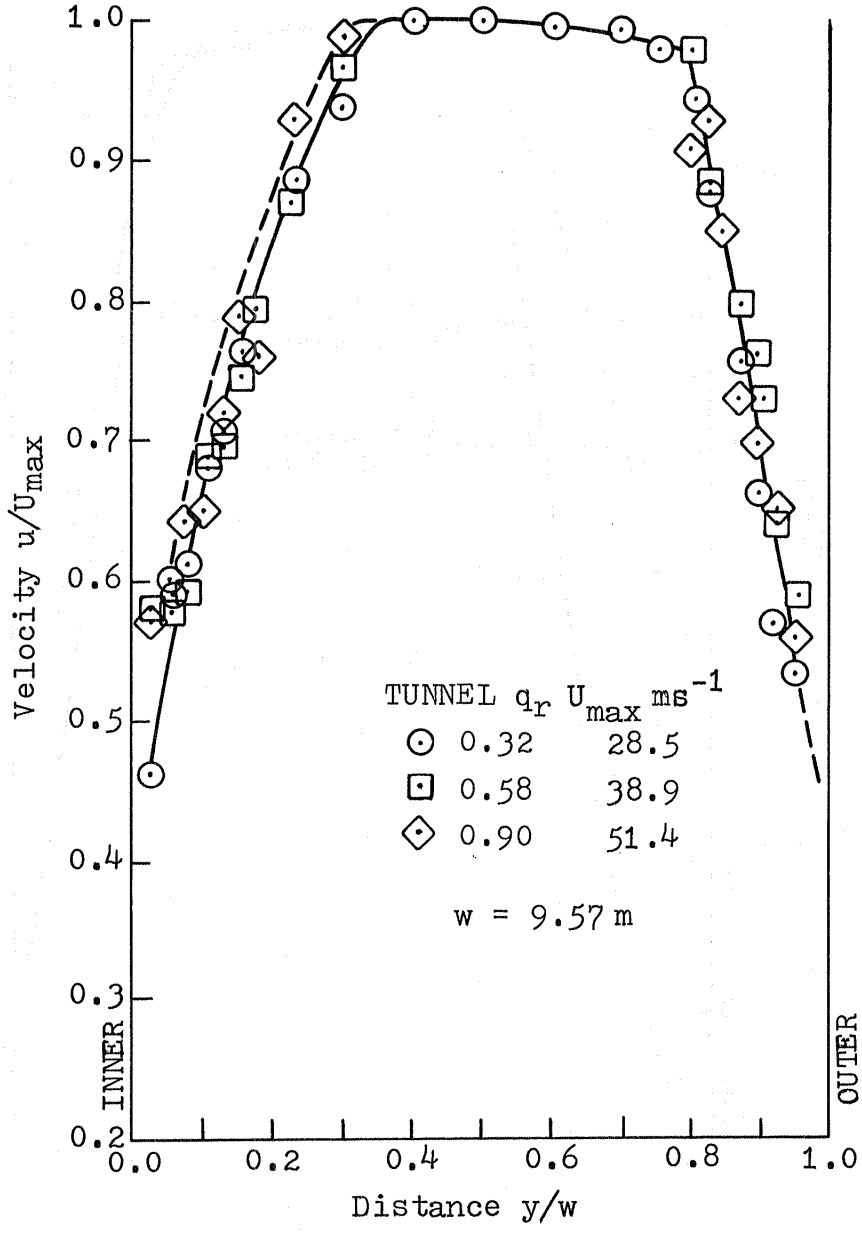


(b) Air breather fully open

Figure 9 Continued

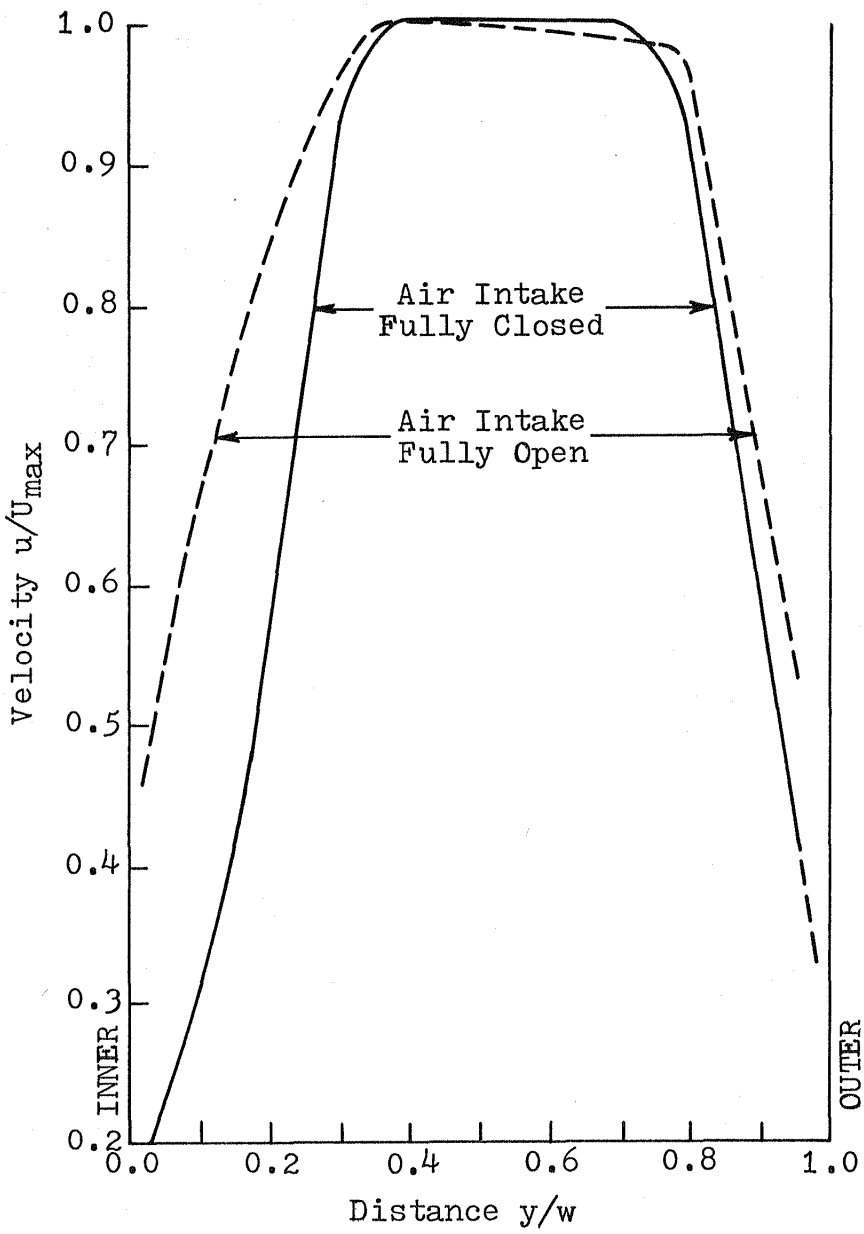


(c) Comparison between fully closed and fully open air breather

Figure 9 Concluded

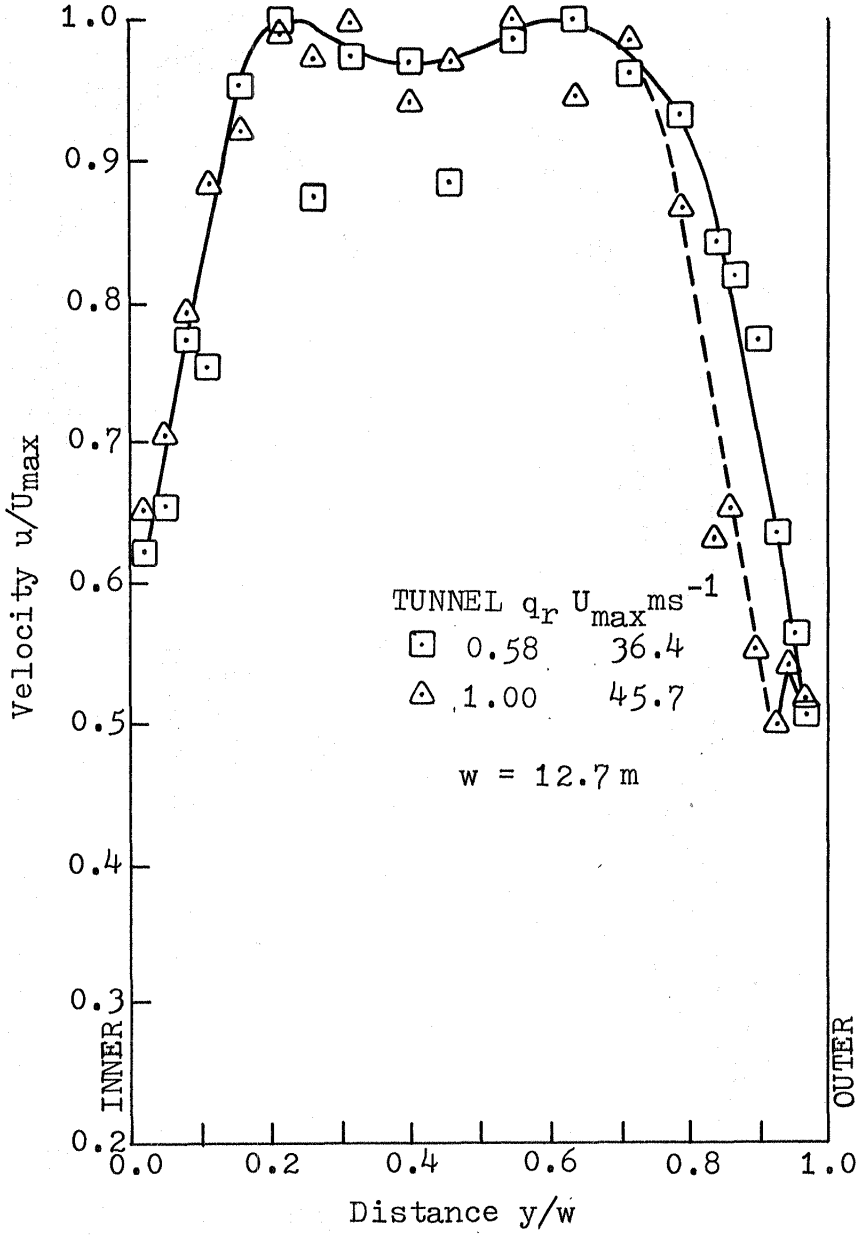


(a) Traverse Station 9A

Figure 10. Velocity distribution in the second diffuser.

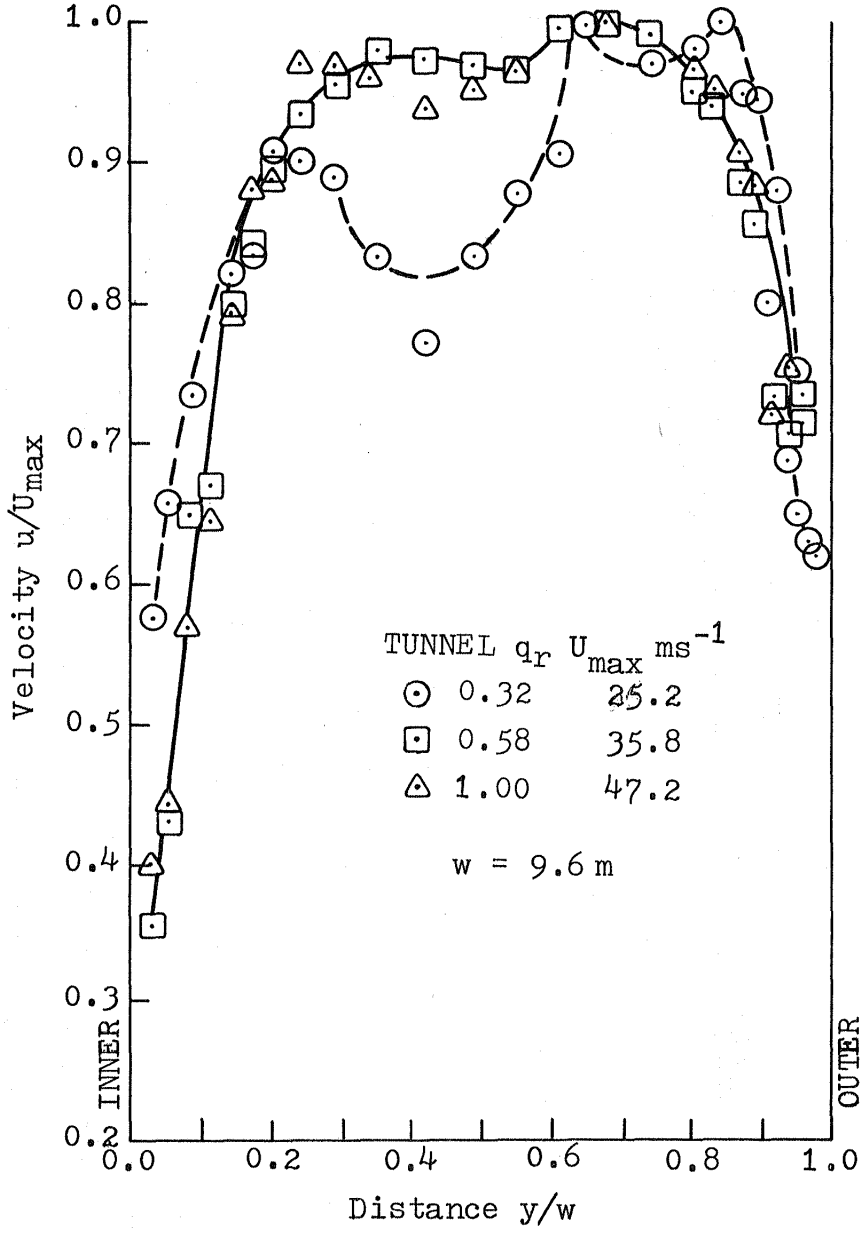


(b) Traverse Station 9B

Figure 10 Continued

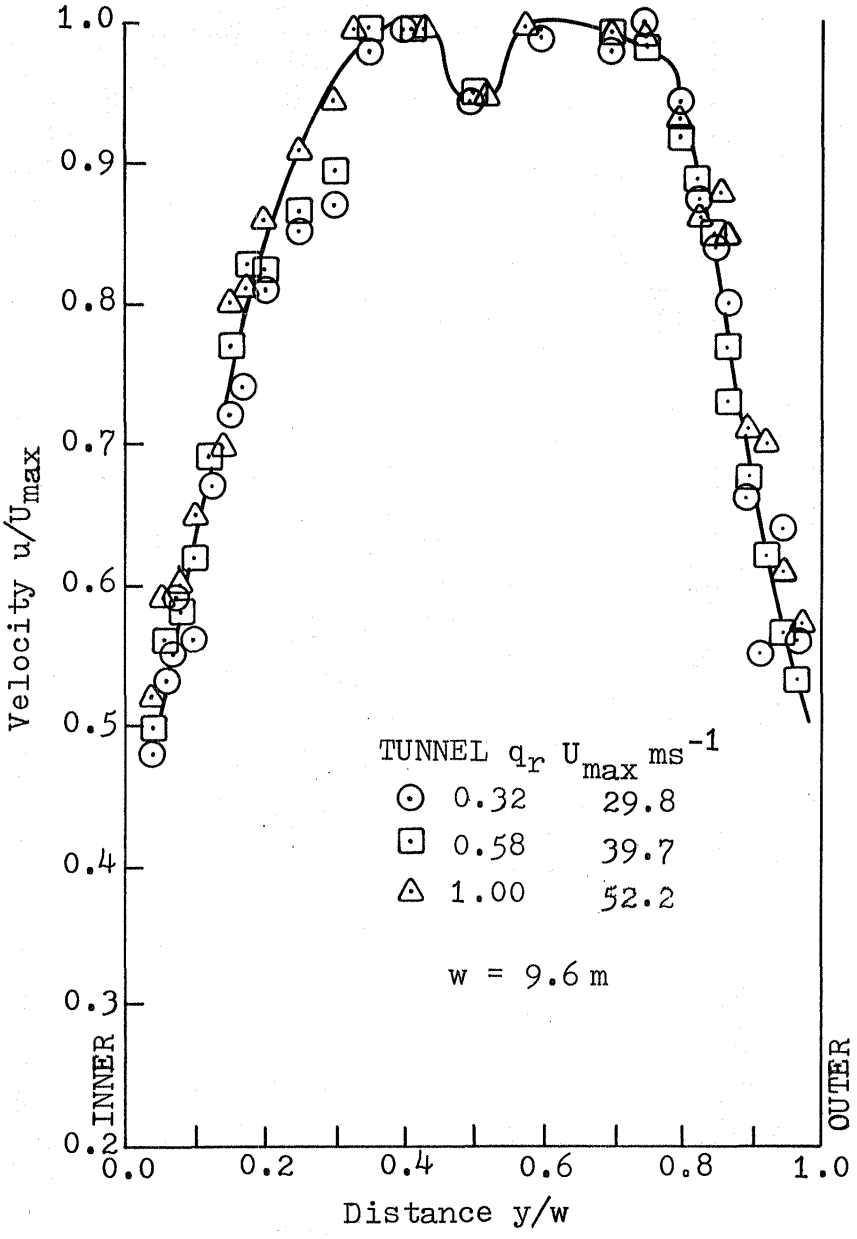


(c) Traverse Station 10A

Figure 10 Concluded

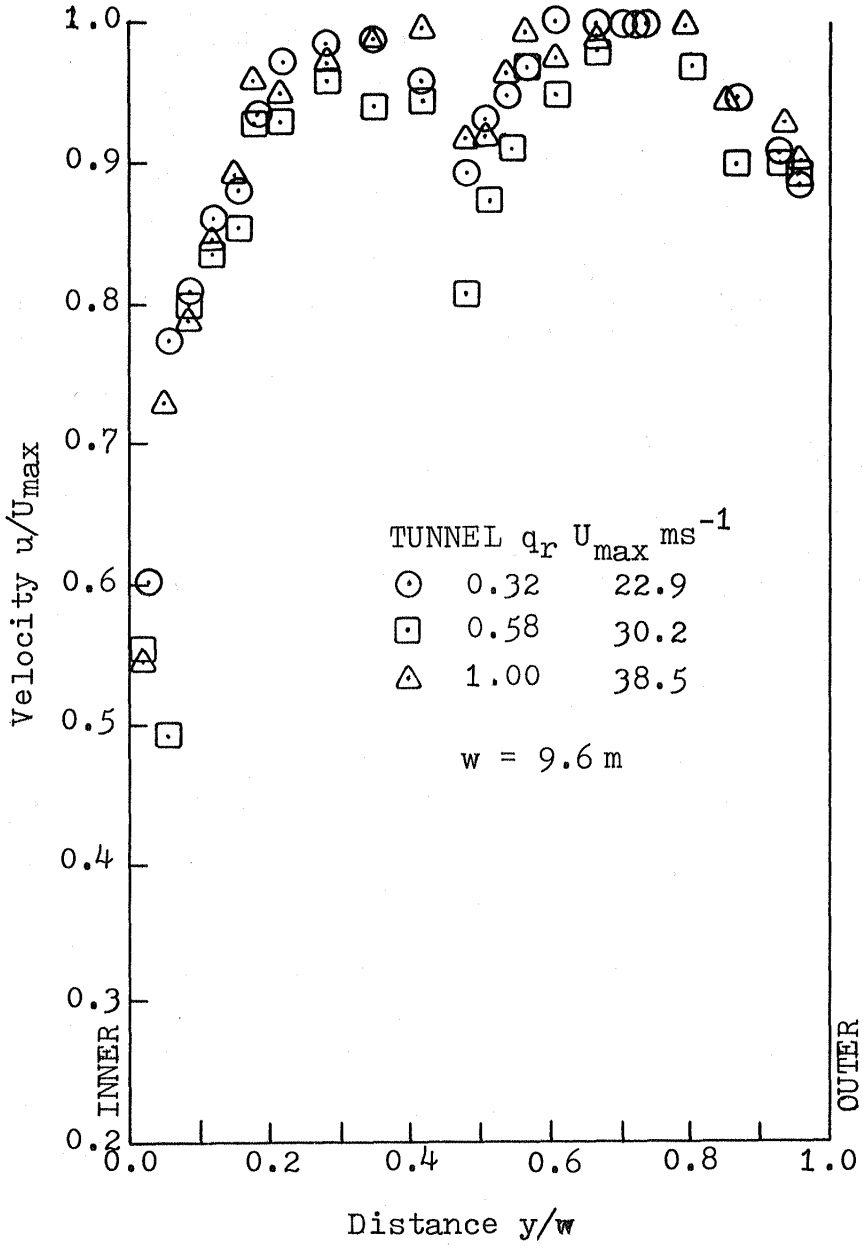


(a) Traverse Station 11

Figure 11. Velocity distribution in the third diffuser.

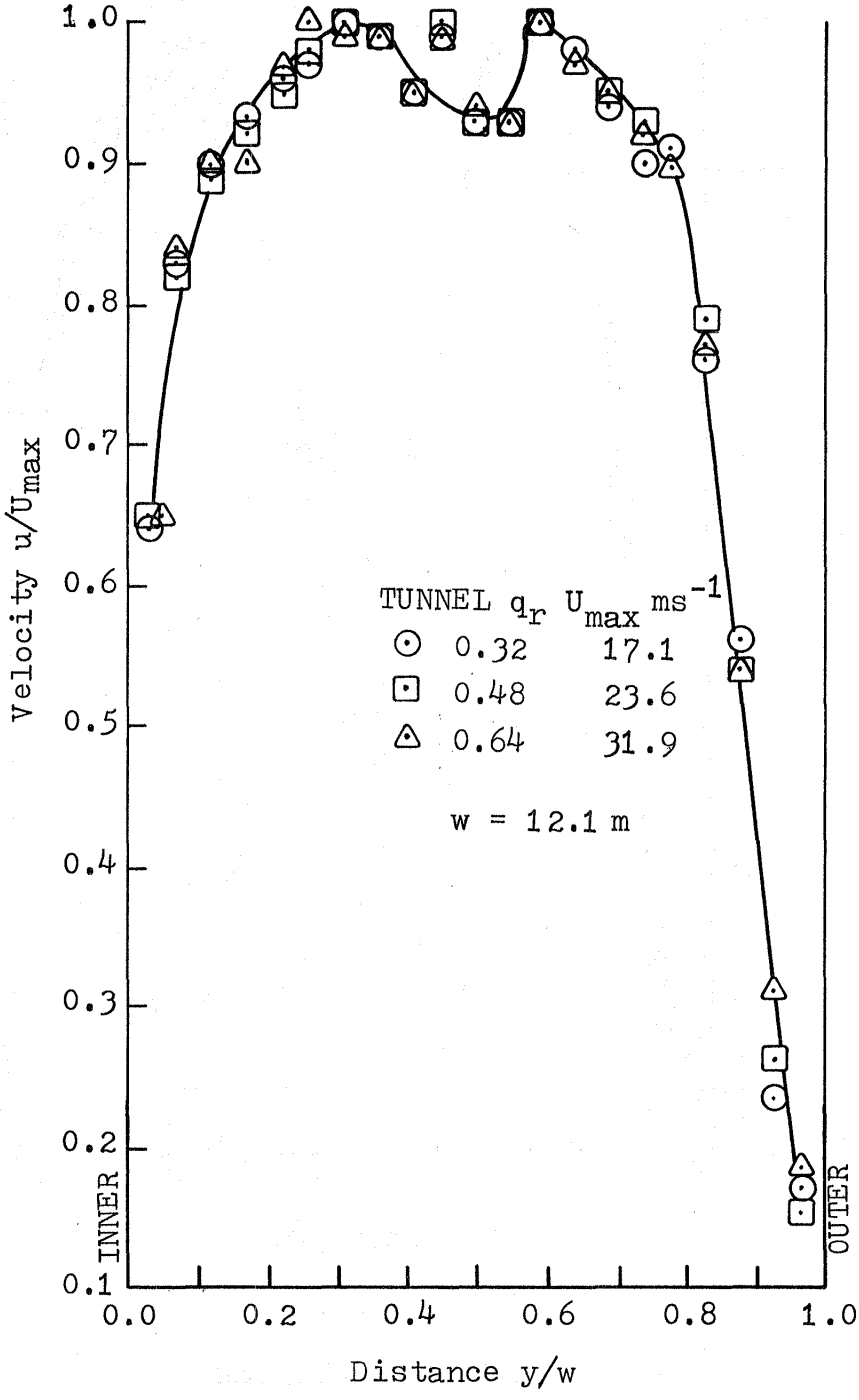


(b) Traverse Station 12

Figure 11 Continued

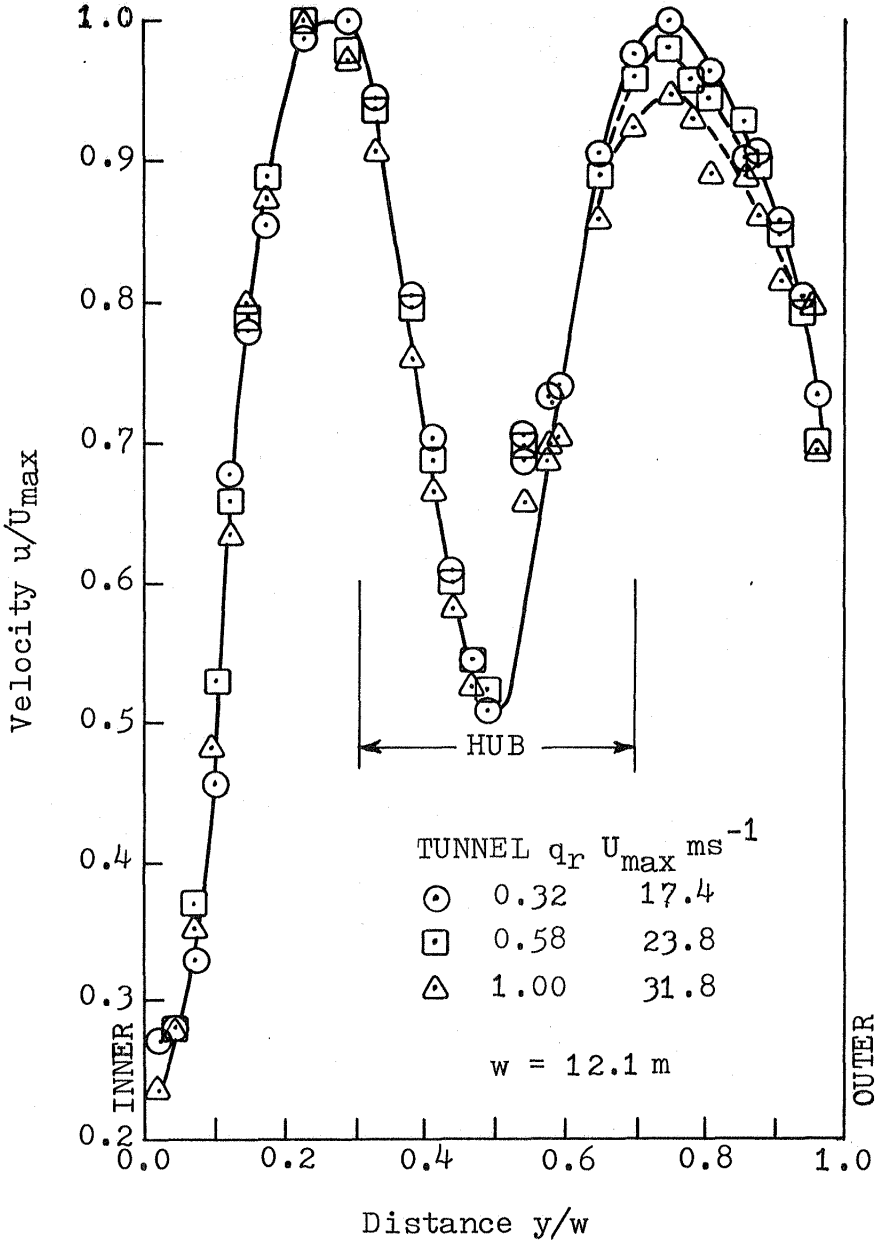


(c) Traverse Station 13

Figure 11 Concluded

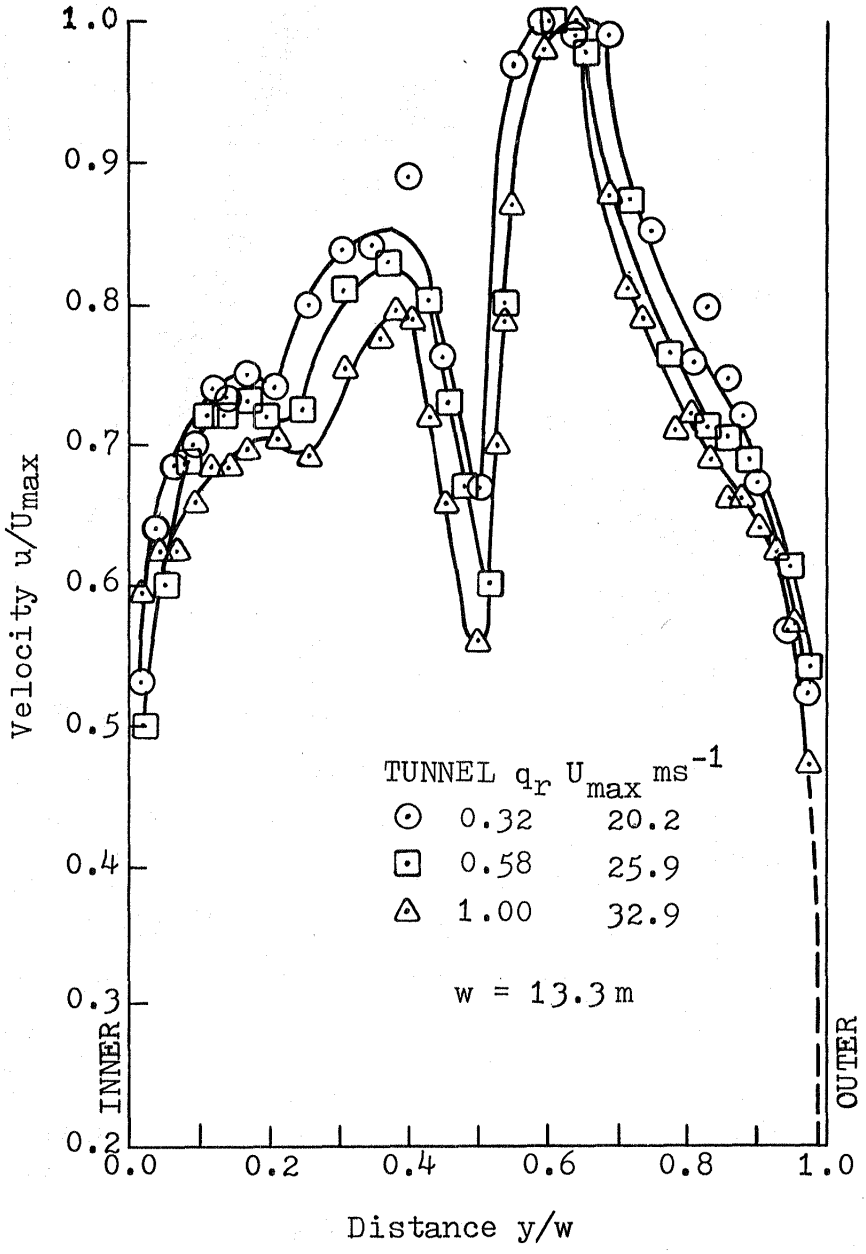


(a) Traverse Station 14

Figure 12. Velocity distribution in the fourth diffuser.

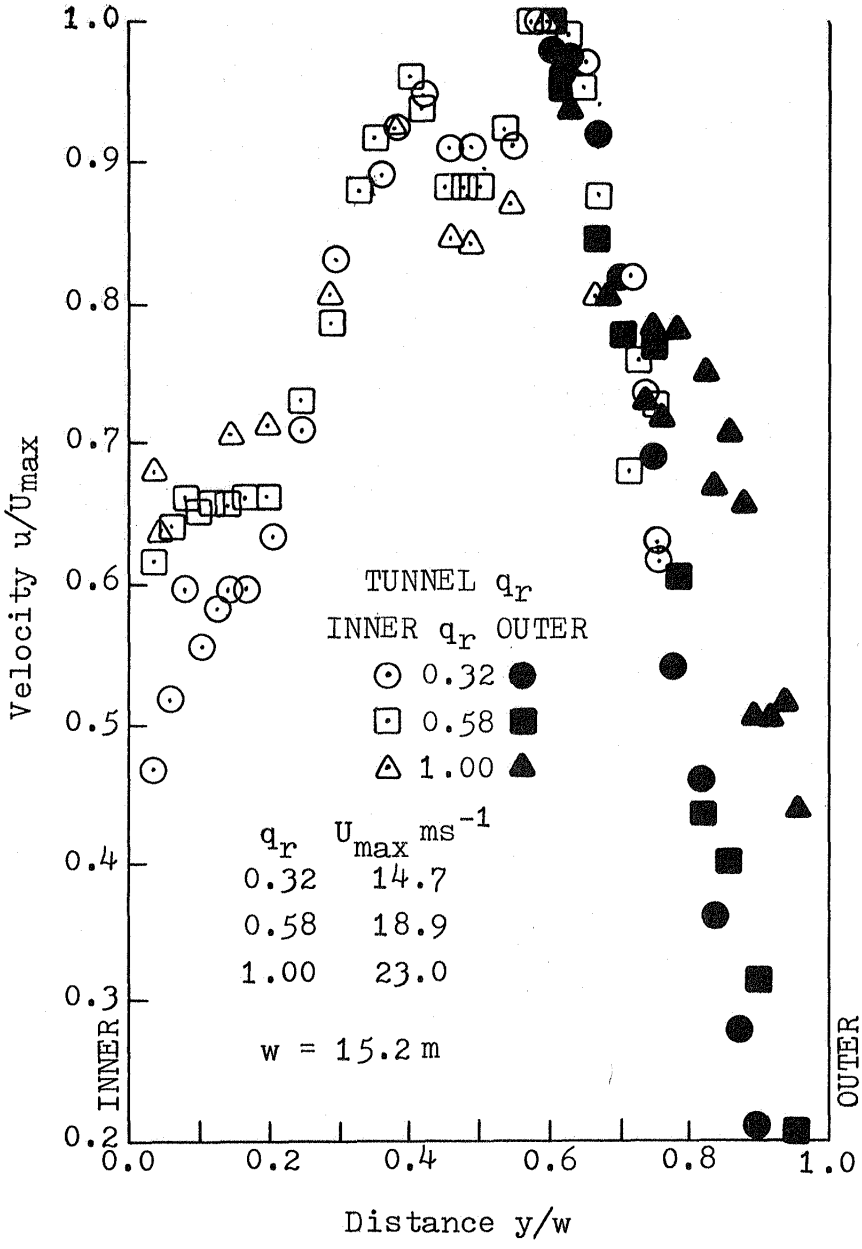


(b) Traverse Station 15

Figure 12 Continued

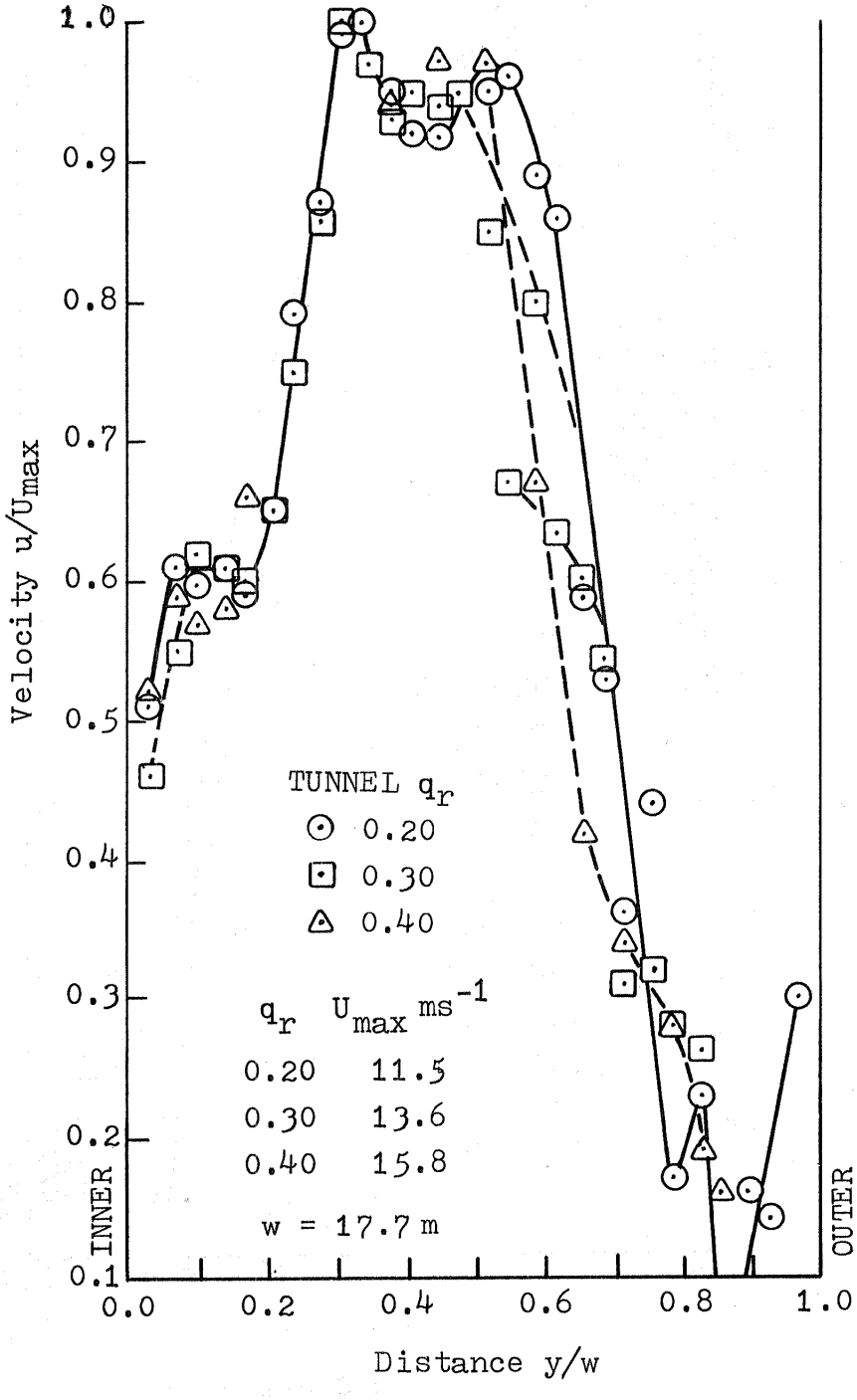


(c) Traverse Station 16

Figure 12 Concluded

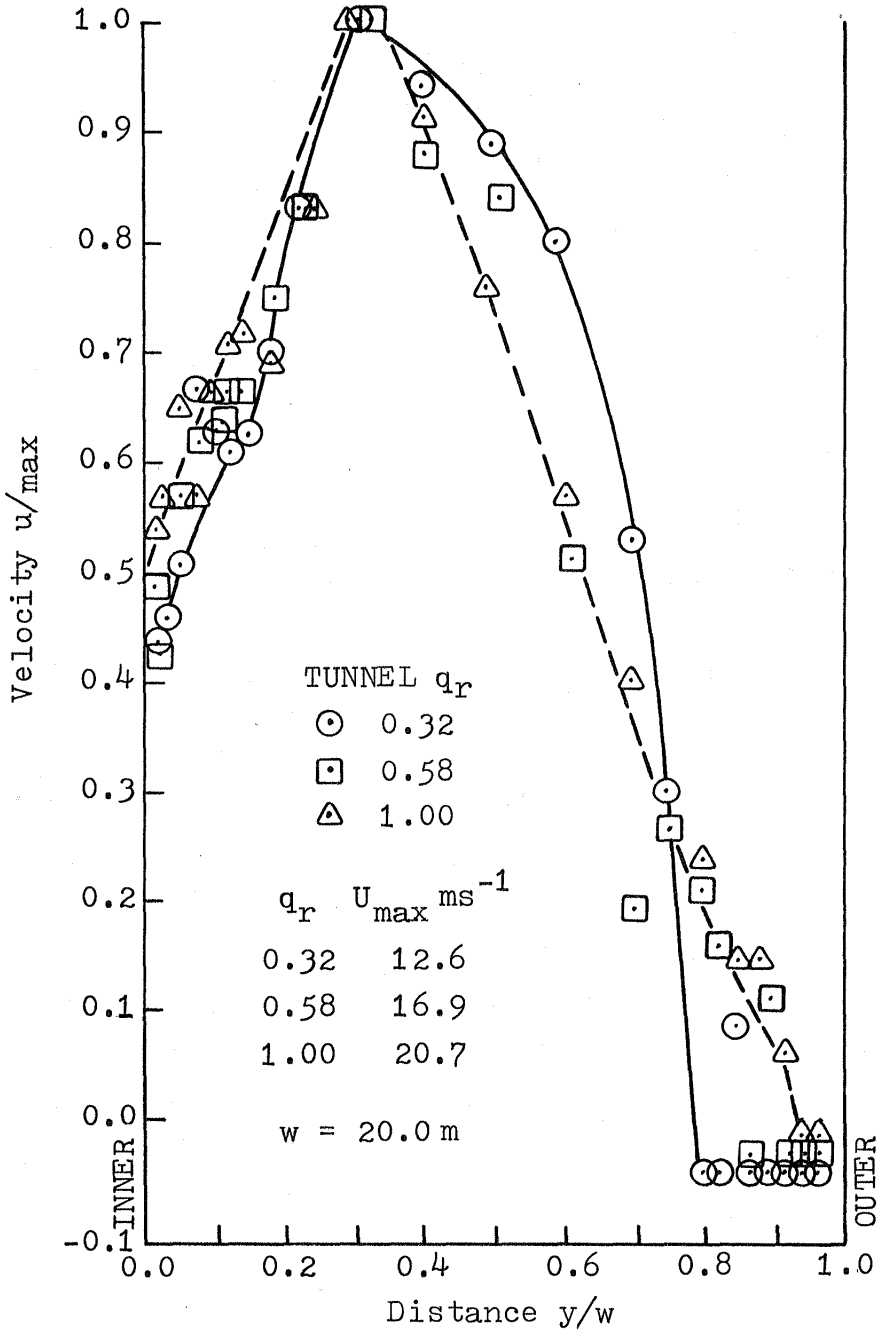


(a) Traverse Station 17

Figure 13. Velocity distribution in sections upstream from the contraction.

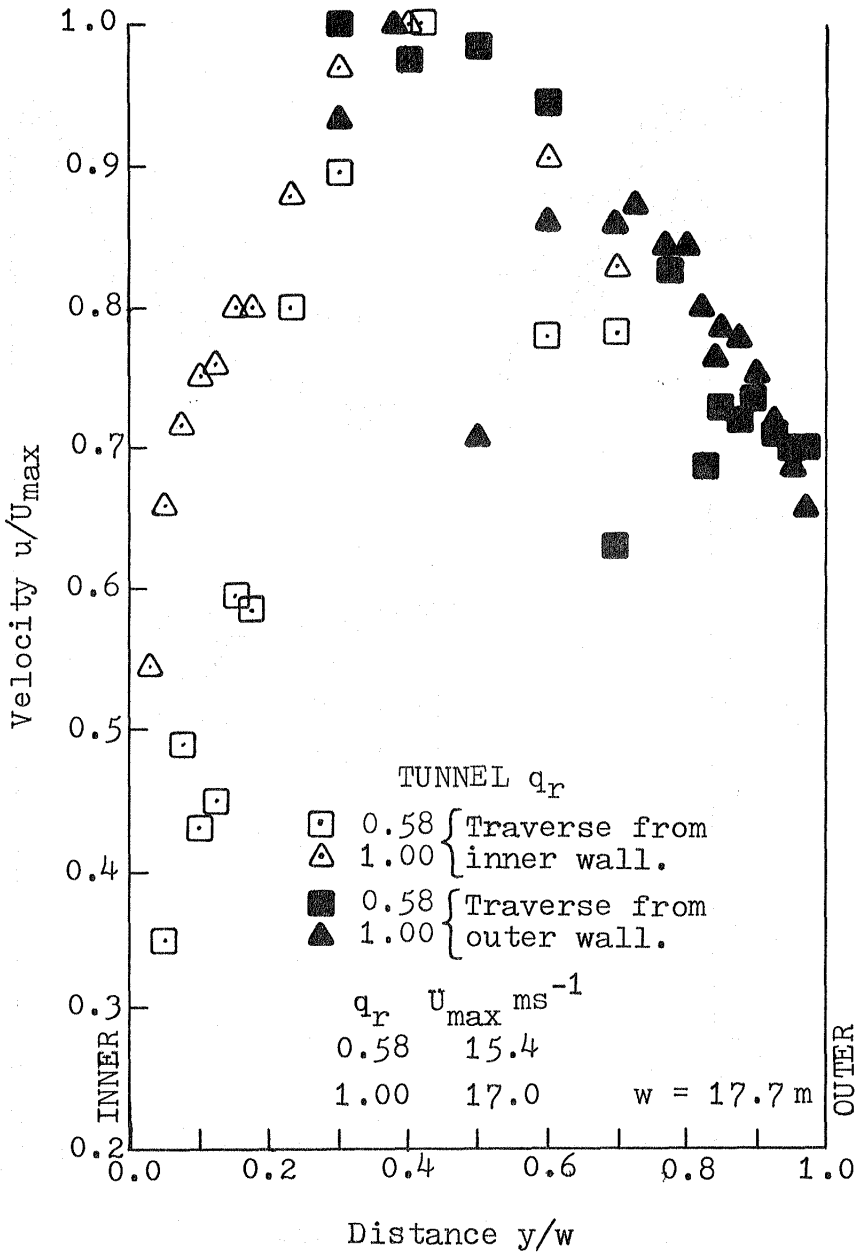


(b) Traverse Station 19

Figure 13 Concluded

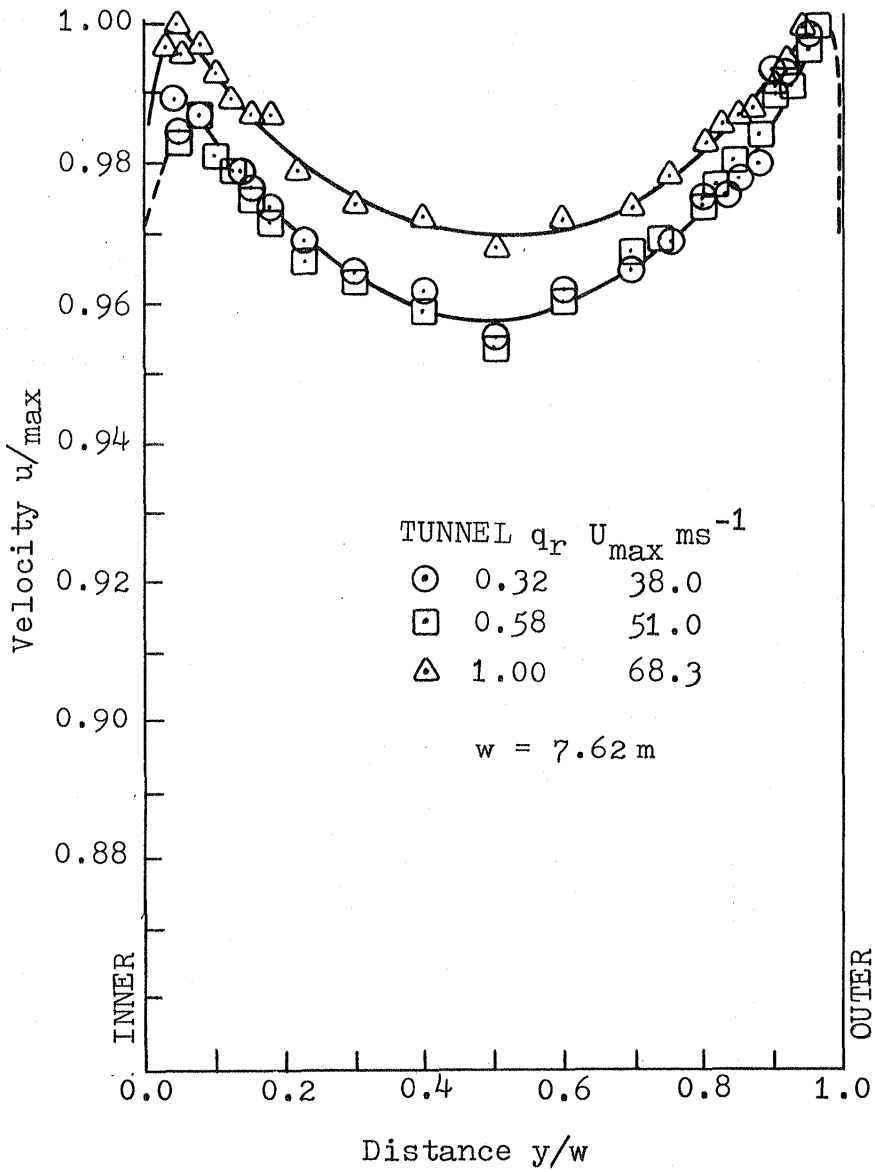


Figure 14. Velocity distribution near the exit from the contraction at T.S.20.

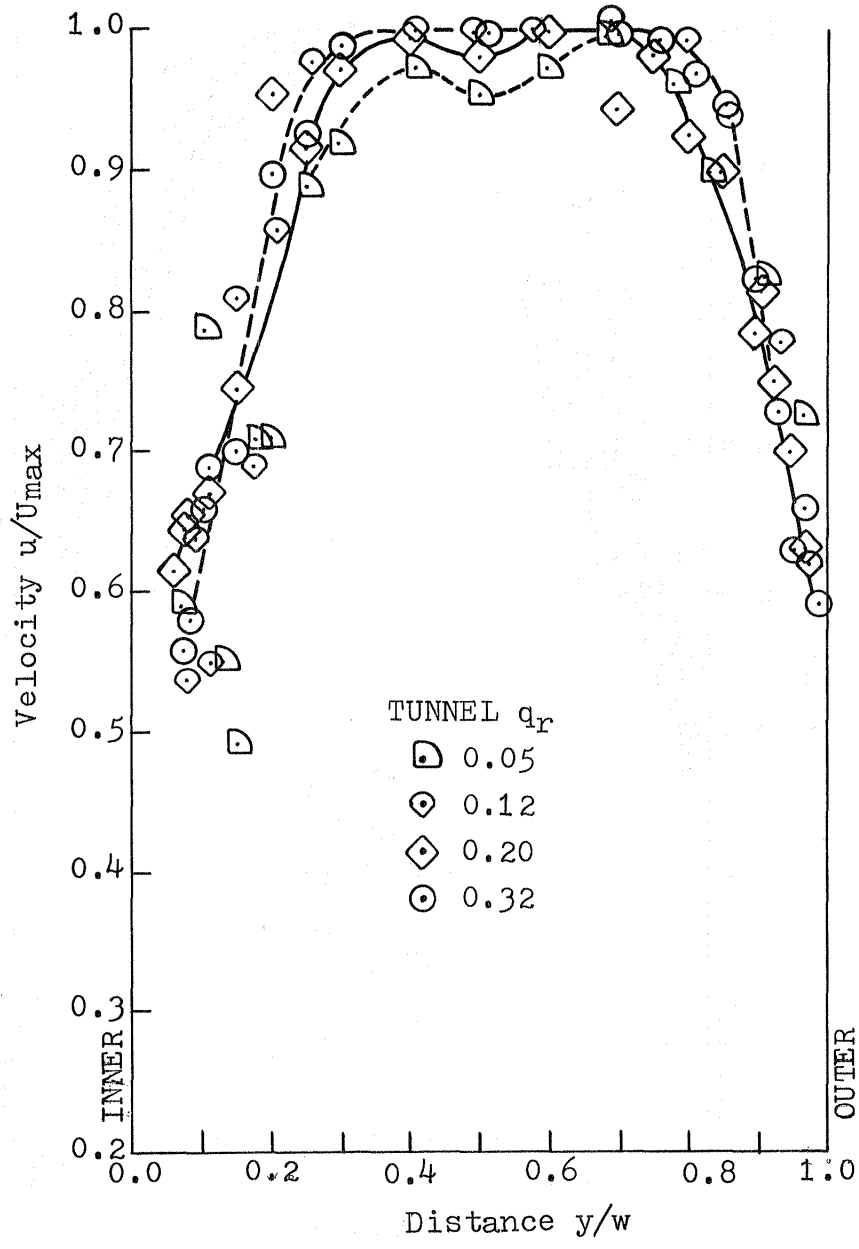


(a) Traverse Station 2

Figure 15. The effects of the open test section on the velocity distribution around the tunnel circuit.

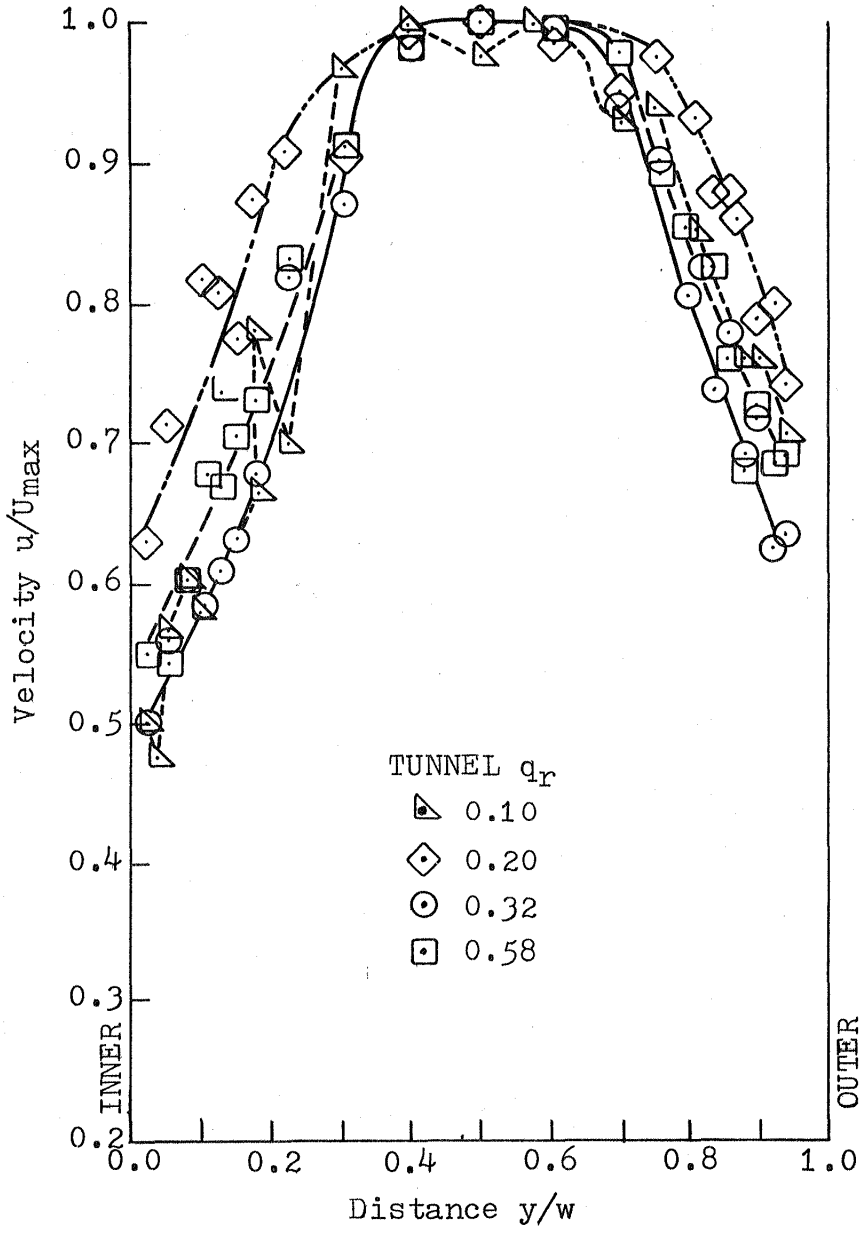


(b) Traverse Station 4

Figure 15 Continued

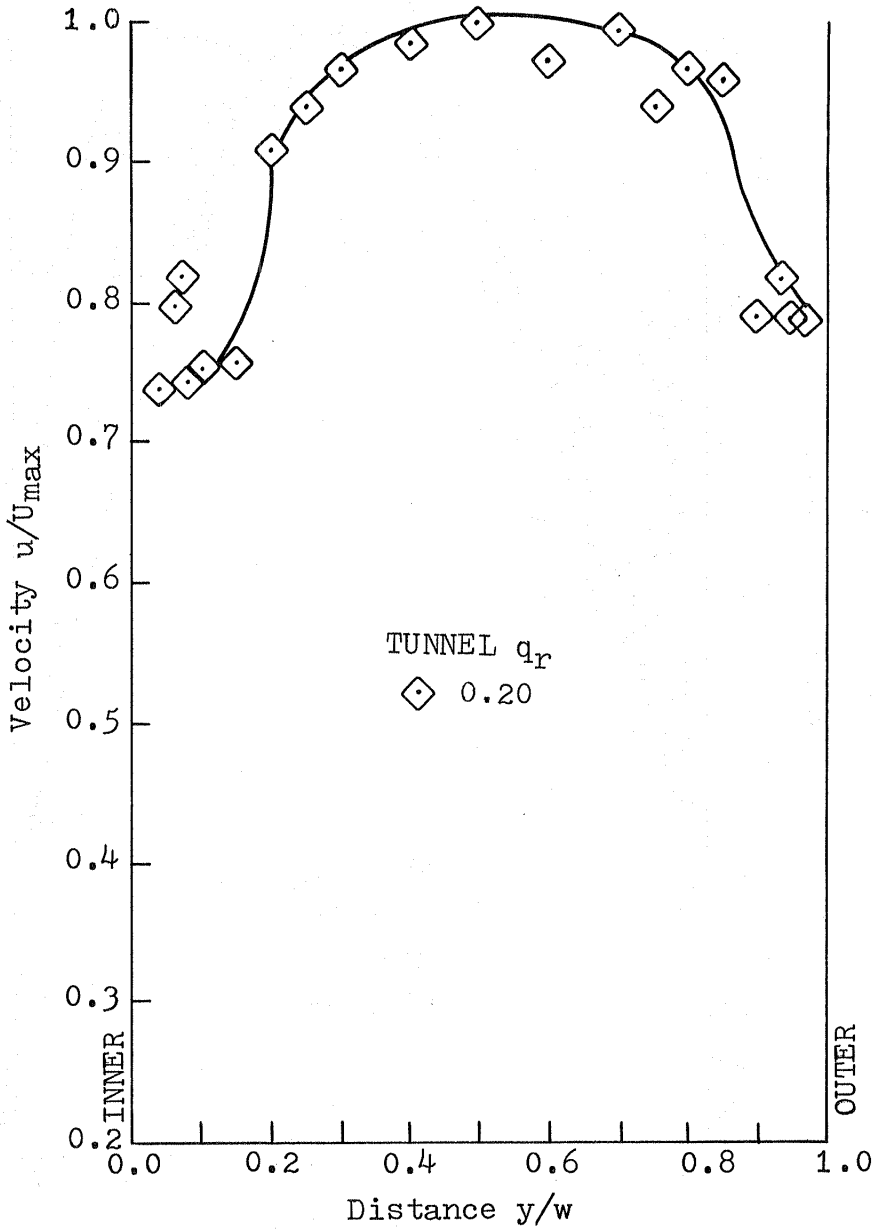


(c) Traverse Station 6

Figure 15 Continued

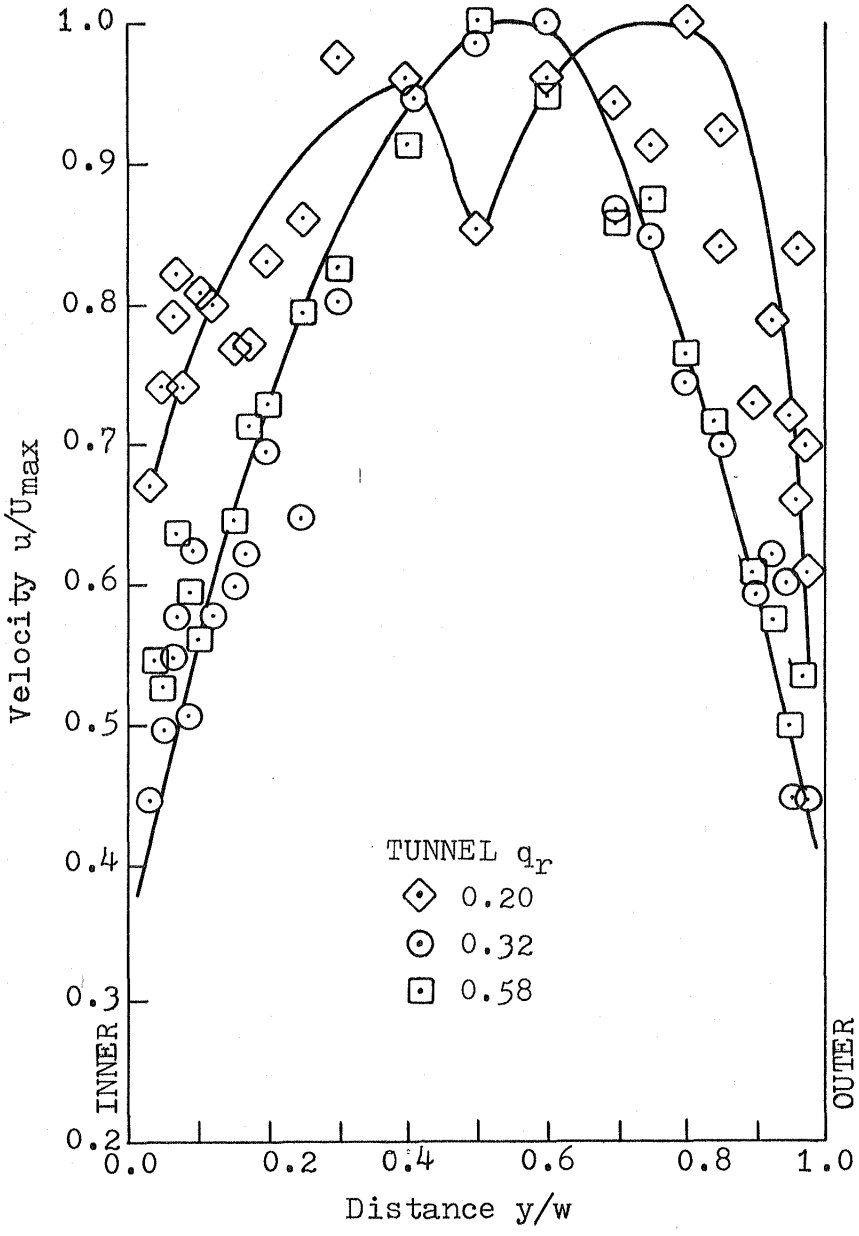


(d) Traverse Station 8A

Figure 15 Continued

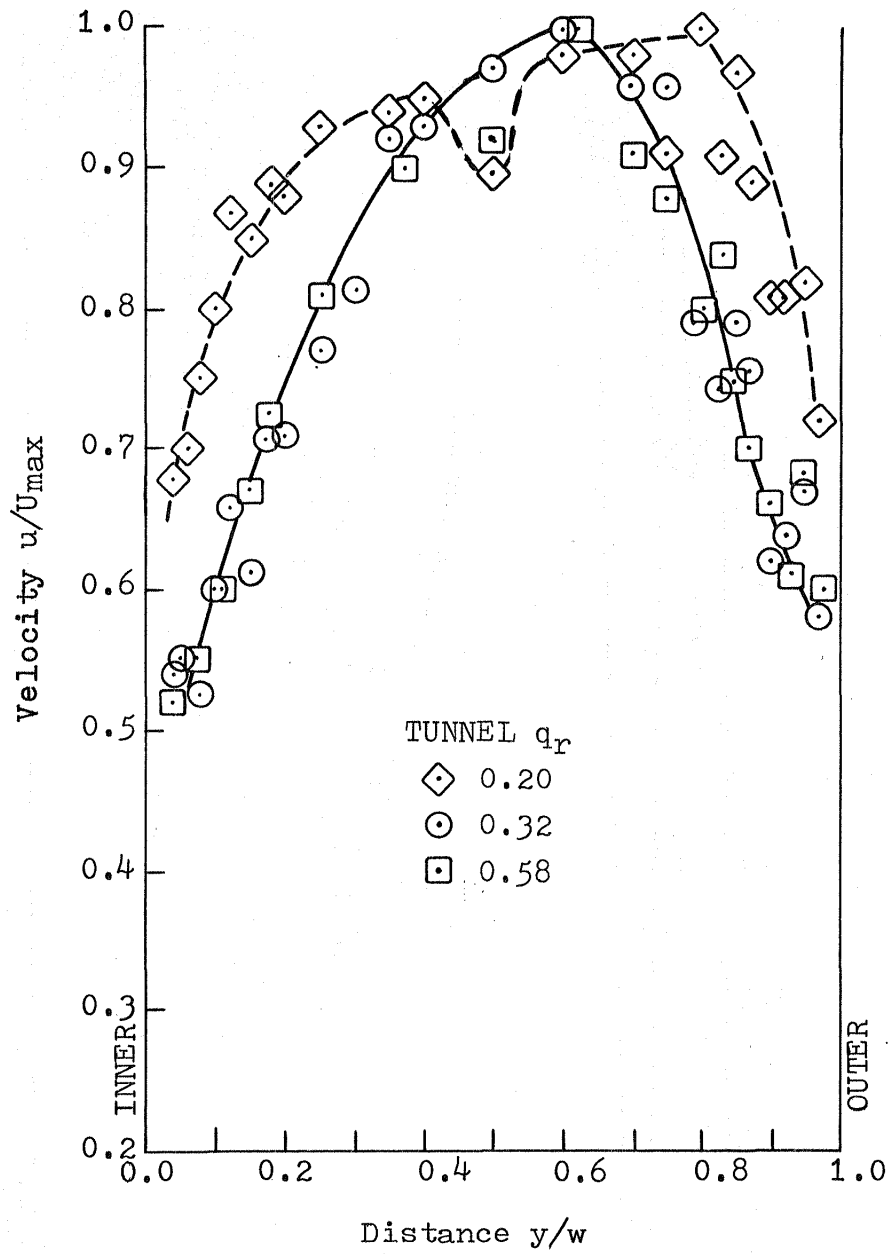


(e) Traverse Station 10A

Figure 15 Continued

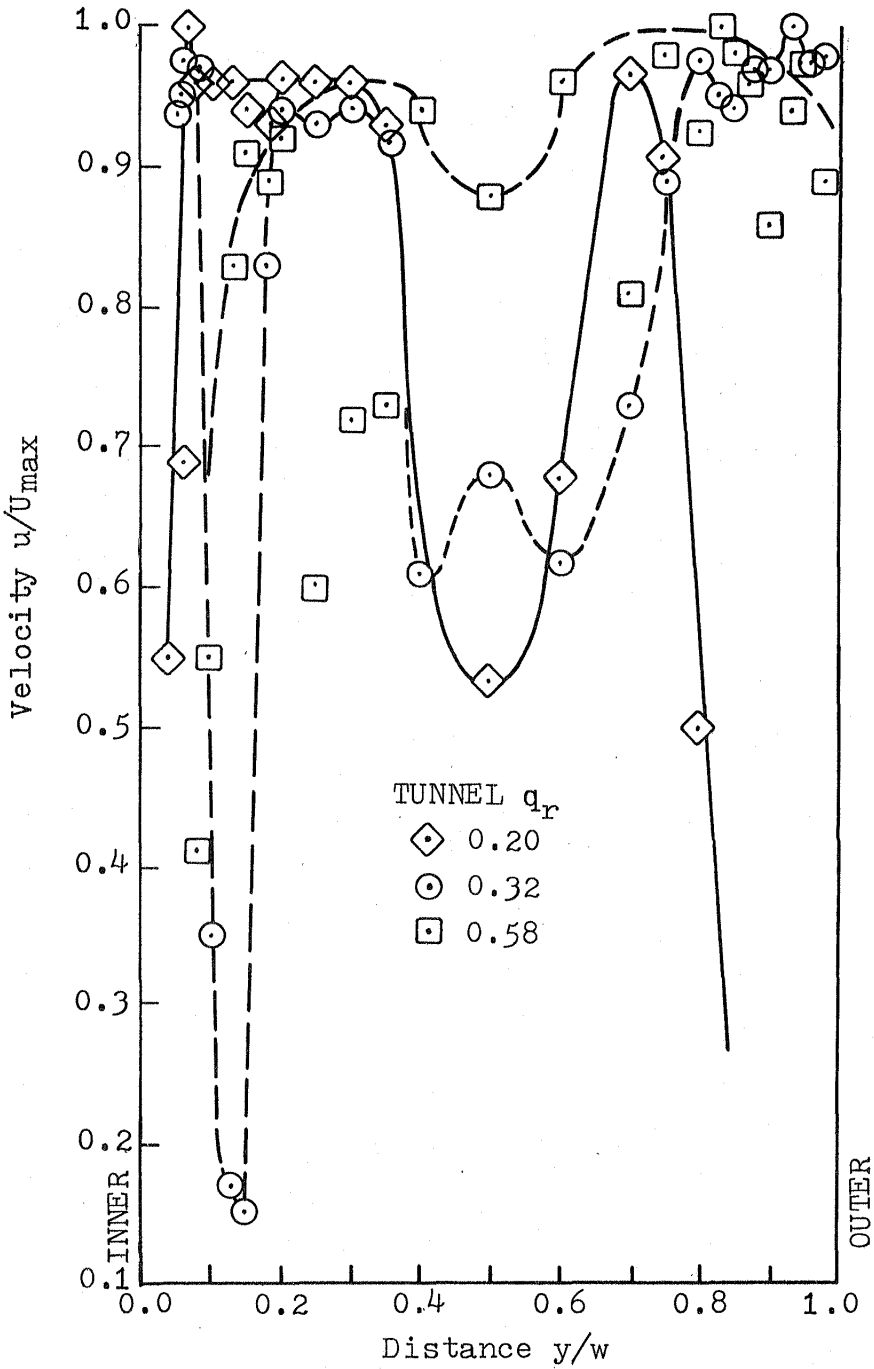


(f) Traverse Station 12

Figure 15 Continued

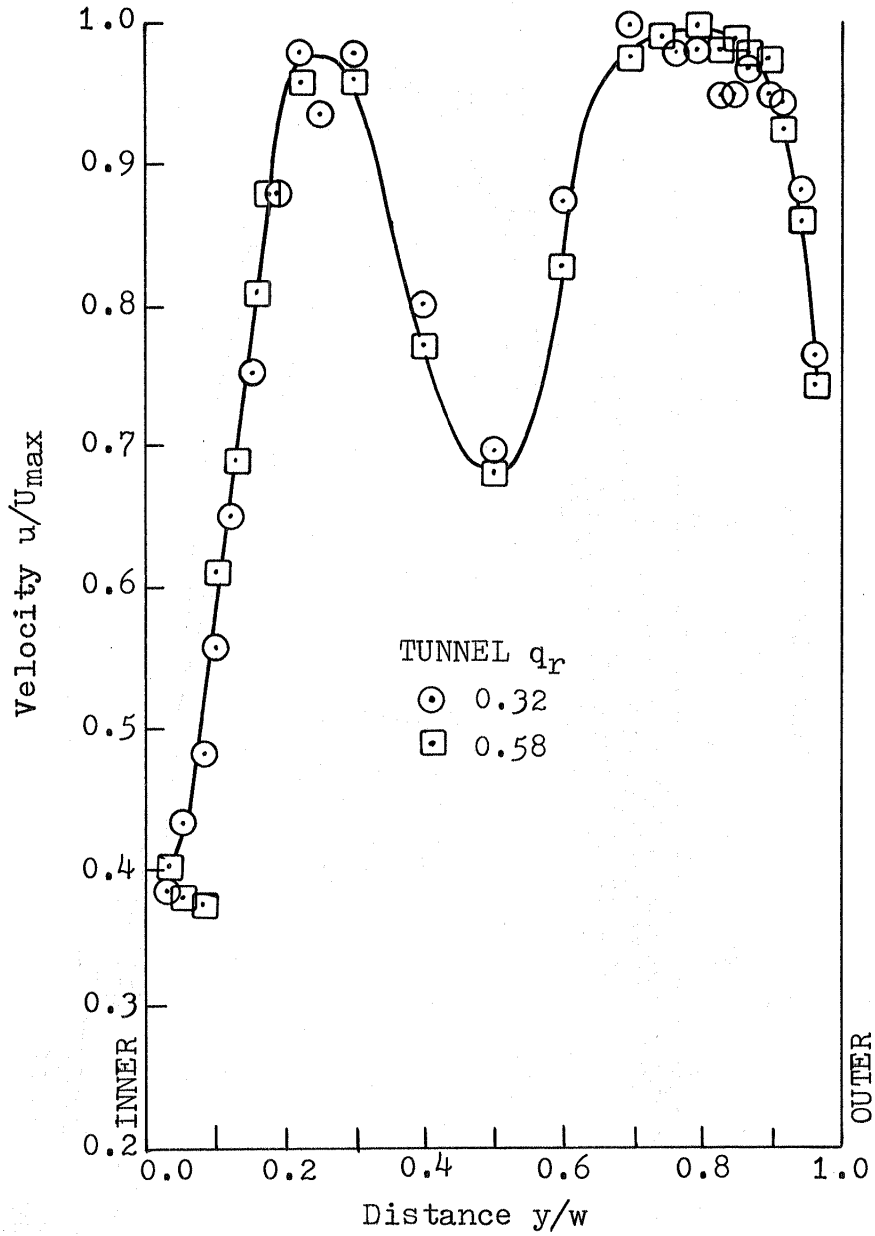


(g) Traverse Station 13

Figure 15 Continued

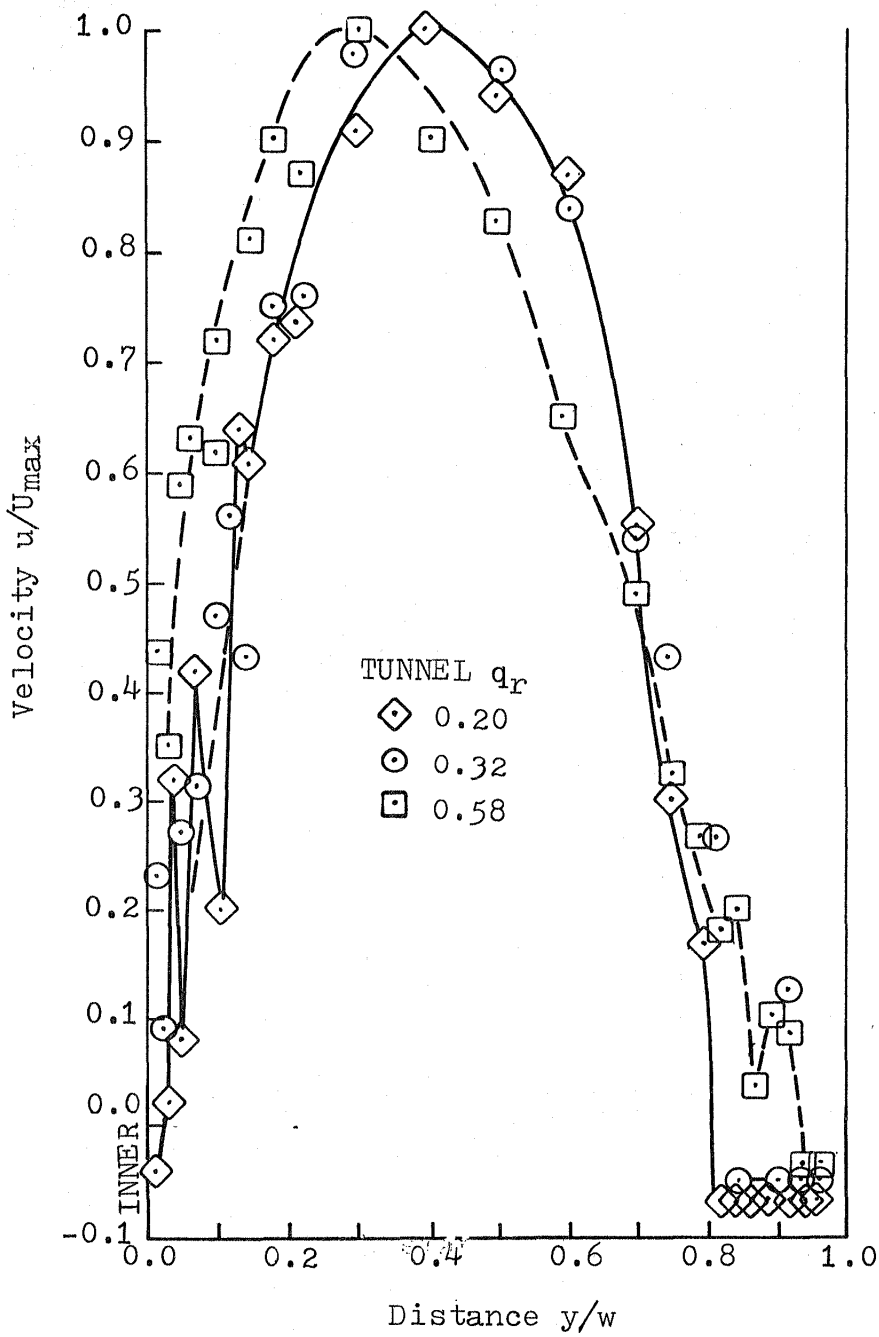


(h) Traverse Station 17

Figure 15 Continued

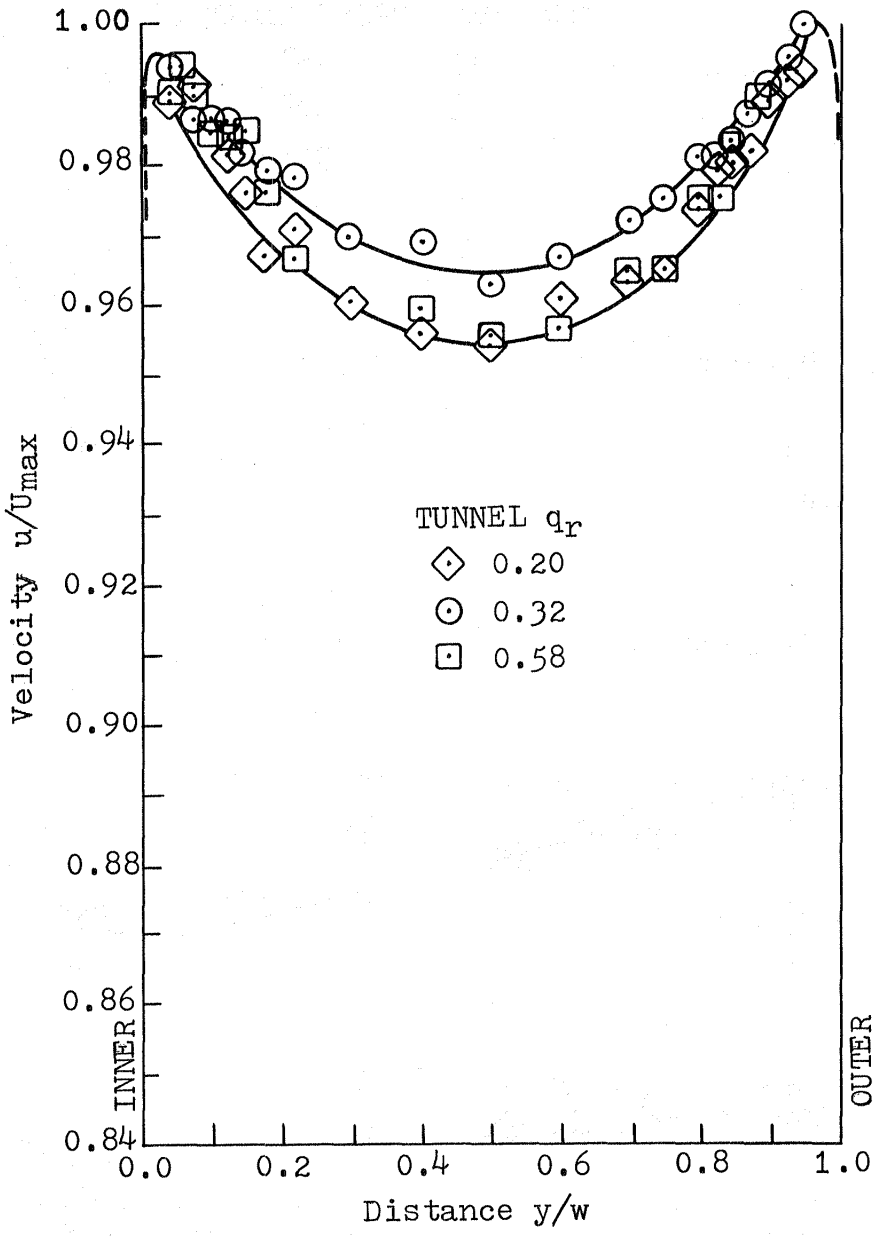


(i) Traverse Station 20

Figure 15 Concluded

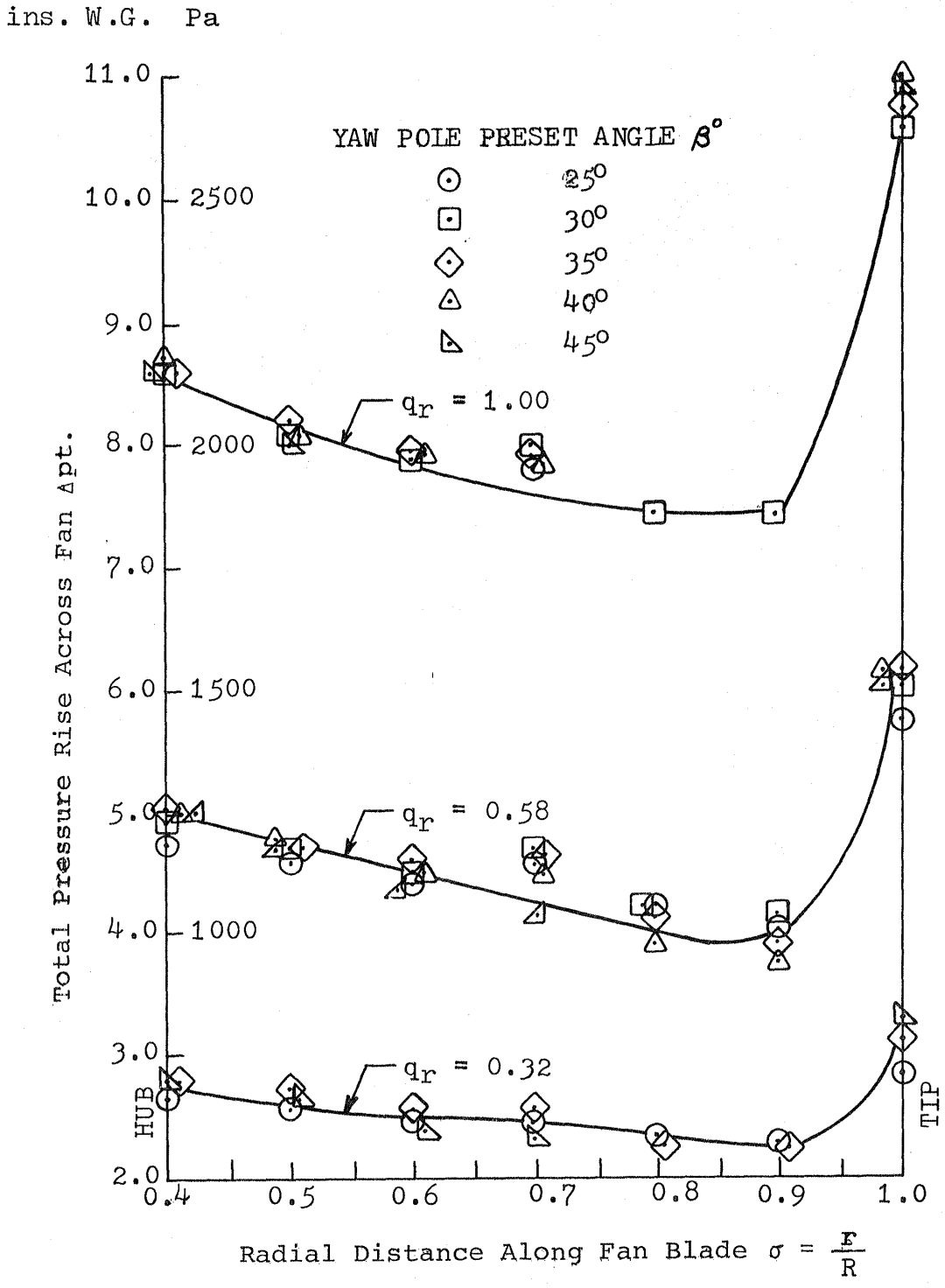


Figure 16. Spanwise variation of total pressure rise across the fan (for various tunnel speeds).

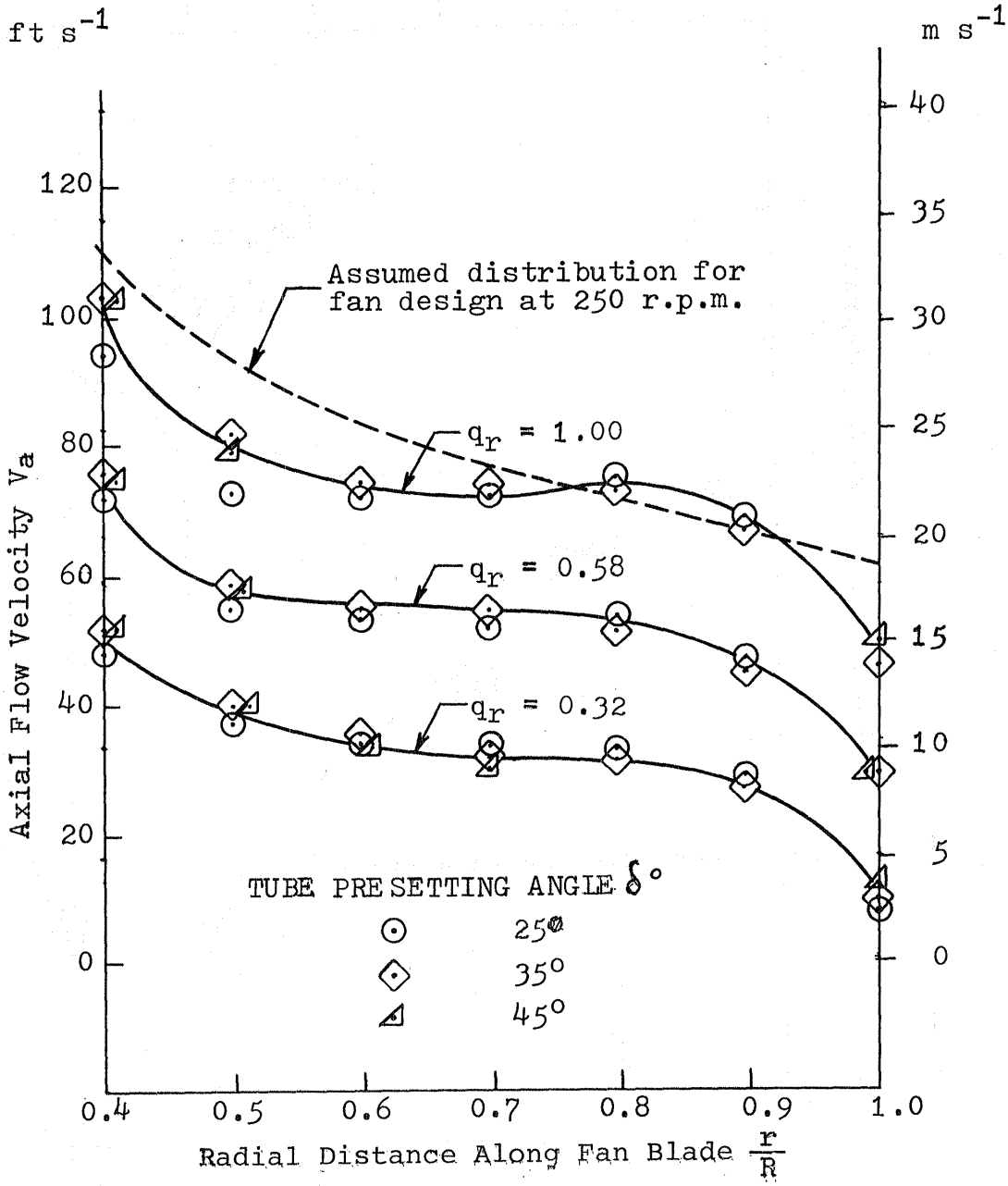


Figure 17. Spanwise variation of axial velocity downstream from the fan (for various tunnel speeds).

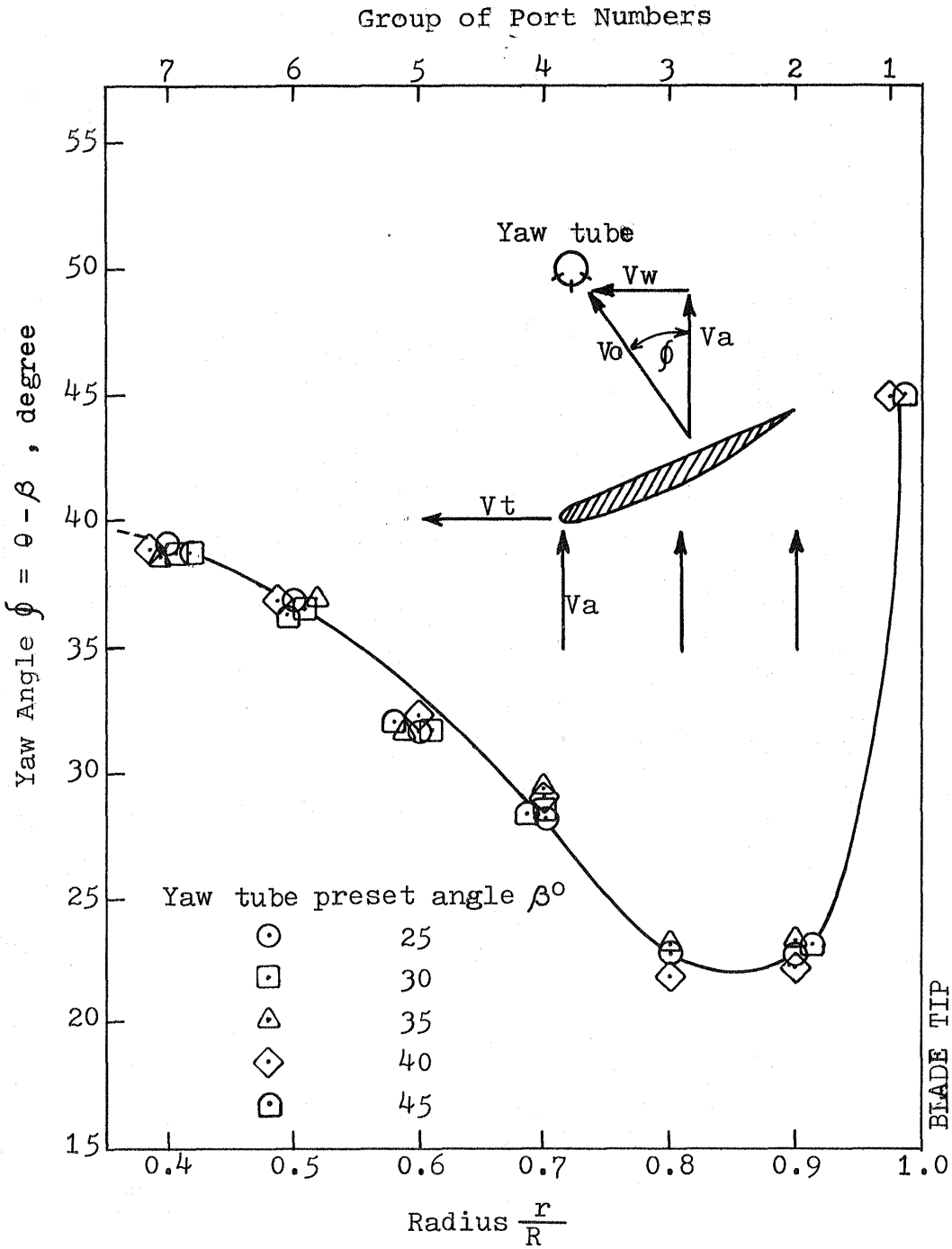


Figure 18. Spanwise variation of yaw angle downstream from fan for various yaw tube preset angles.

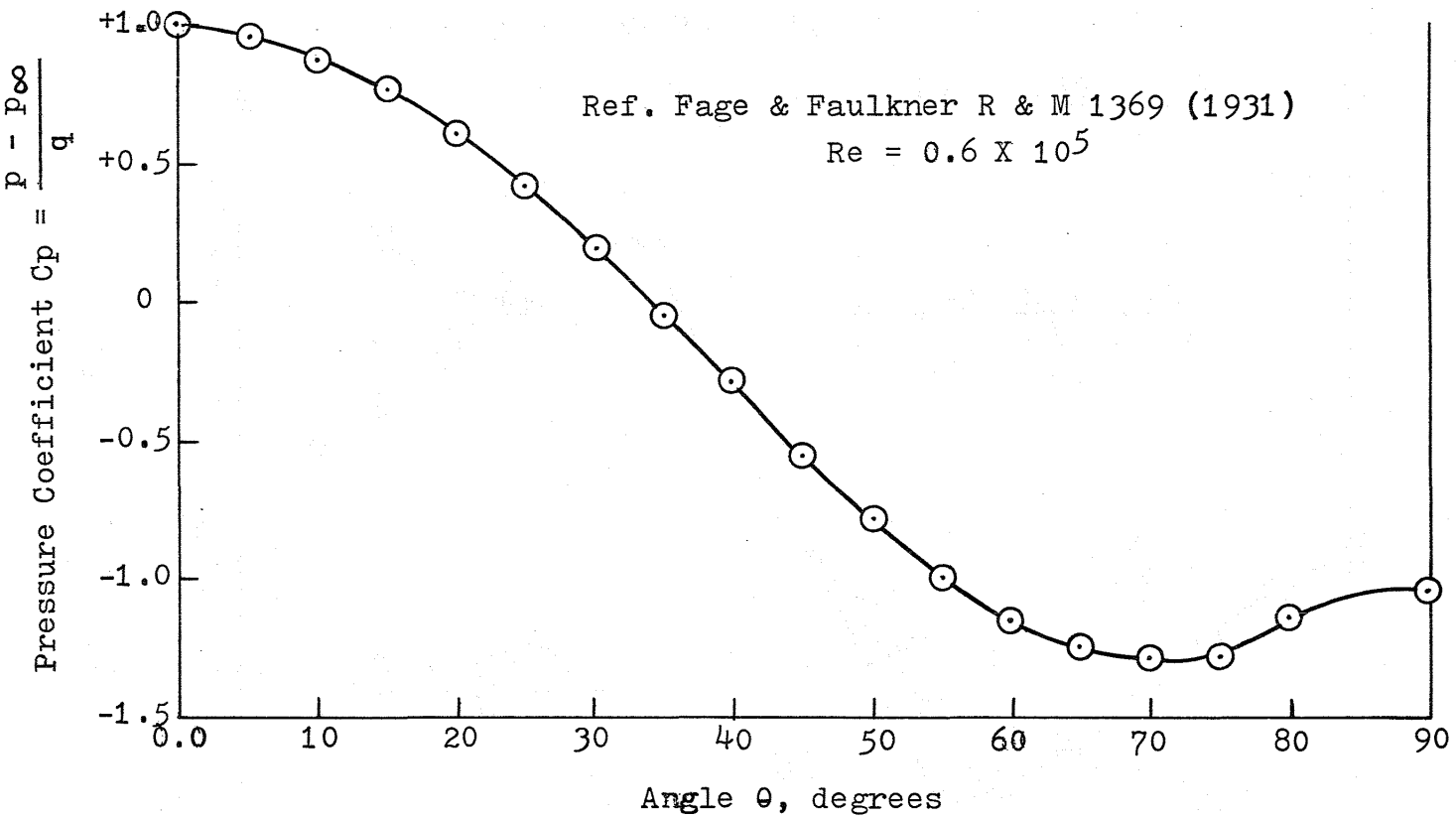


Figure19 . Variation of pressure coefficient with angle of attack around a circular cylinder at Reynolds number $R_e$=0.6x10$^5$.

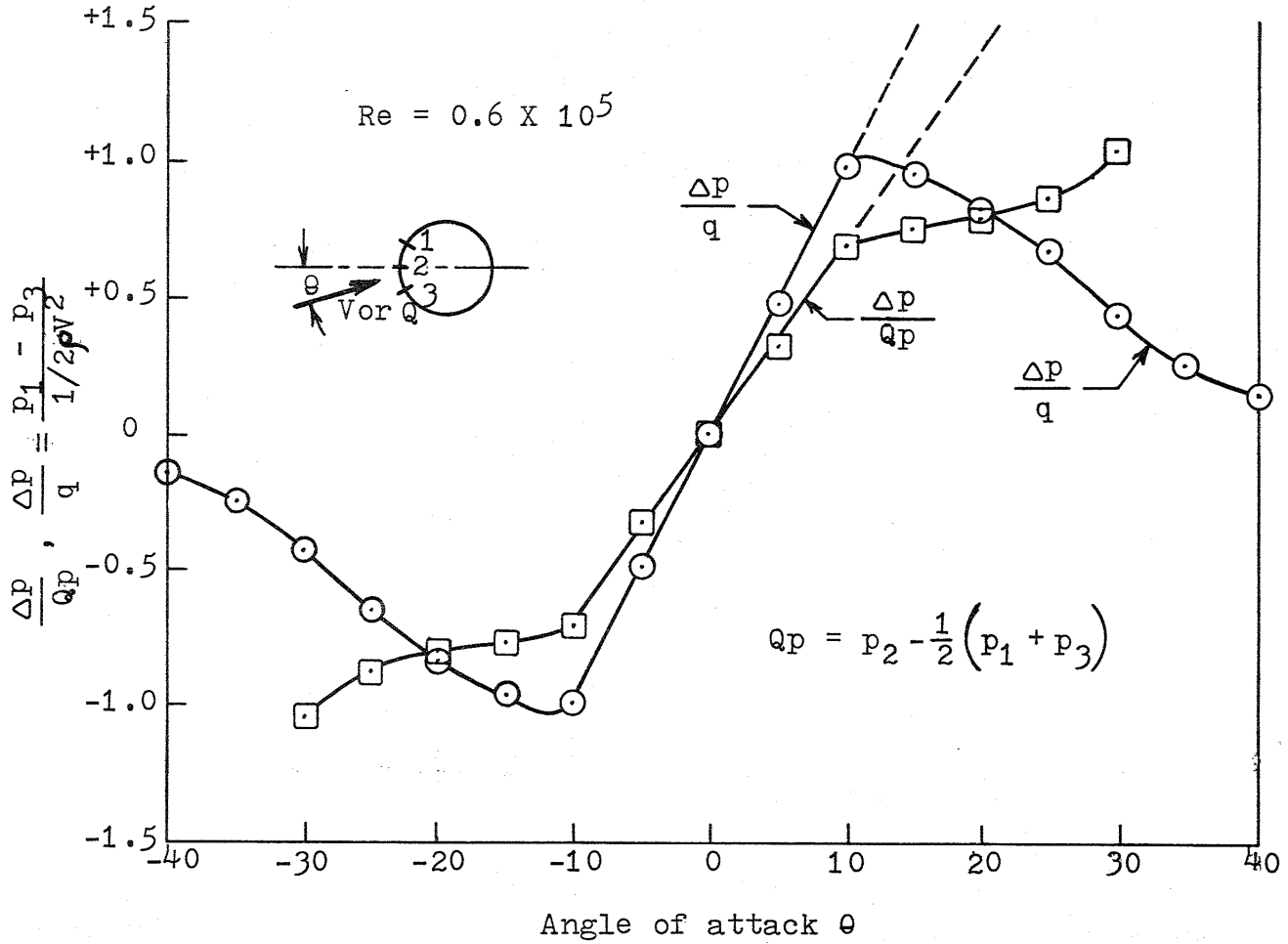


Figure 20. Variation of pressure differentials between ports with angle of attack.

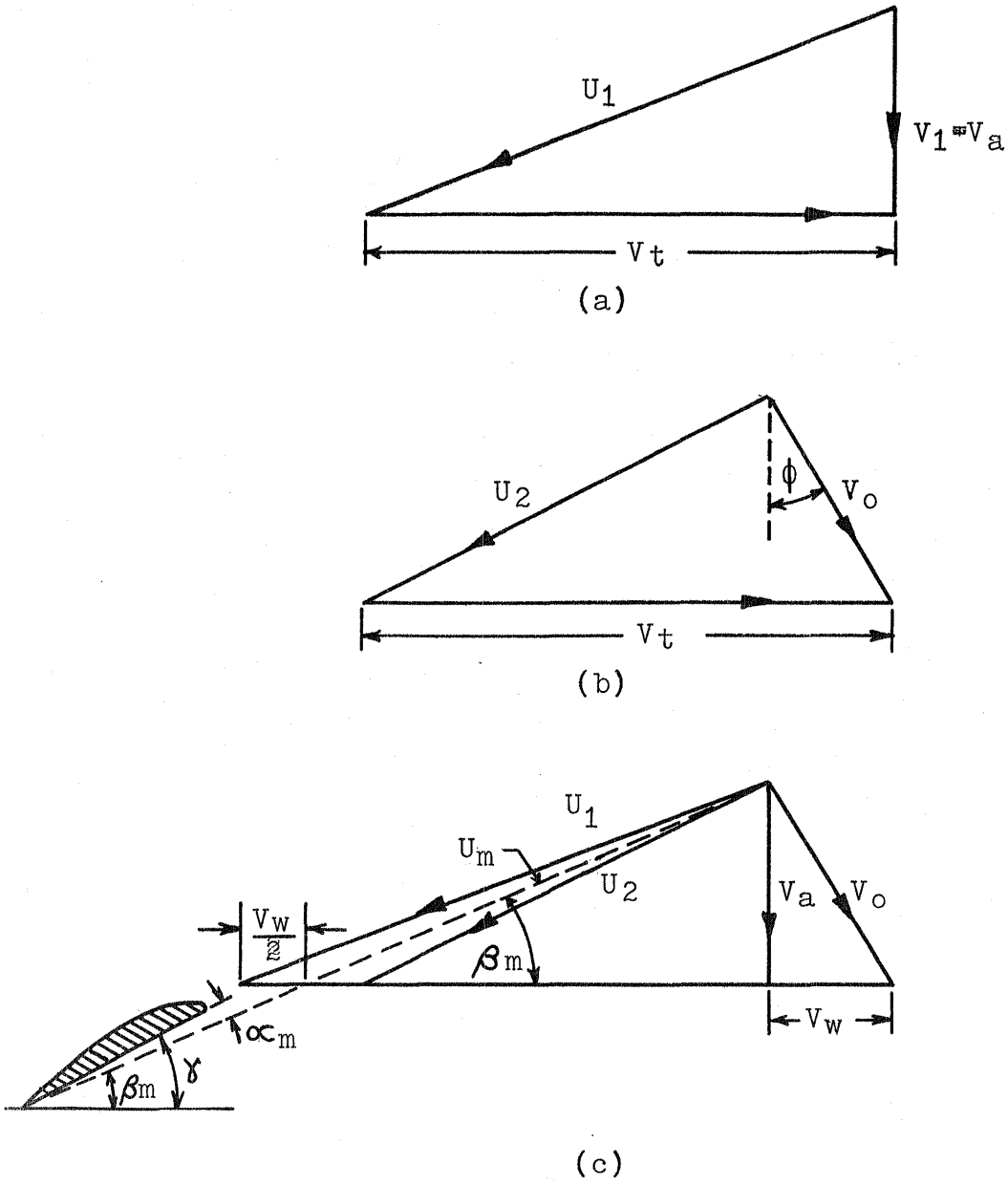


Figure 21. Velocity vector diagrams of a flow through a fan.

| 1. Report No. | 2. Government Accession No. | 3. Recipient's Catalog No. |
|---|---|---|
| NASA CR-165655 | | |

| 4. Title and Subtitle | 5. Report Date |
|---|---|
| Experimental Investigations on the V/STOL Tunnel at NASA/Langley Research Center | February 1981 |
| | 6. Performing Organization Code |
| 7. Author(s) | 8. Performing Organization Report No. |
| P. Stephen Barna | |
| | 10. Work Unit No. |
| 9. Performing Organization Name and Address | |
| P. Stephen Barna, Consultant<br>1049 N. Lexan Crescent<br>Norfolk, VA 23508 | 11. Contract or Grant No.<br>L-12343B |
| | 13. Type of Report and Period Covered |
| 12. Sponsoring Agency Name and Address | Contractor report |
| National Aeronautics and Space Administration<br>Hampton, Virginia 23665 | 14. Sponsoring Agency Code |

15. Supplementary Notes

Langley Technical Monitor: Richard J. Margason

16. Abstract

An investigation into the flow characteristics of the V/STOL tunnel at NASA Langley Research Center has been conducted. The results of the investigations show an interaction between tunnel components. The test results show that the flow around the tunnel circuit gradually deteriorated with increasing distance from the testing area. At the beginning of the circuit, the flow in the first diffuser was still satisfactory; at the end of the circuit, the flow approaching the contraction had become entirely unsatisfactory. Deterioration of flow was due largely to turning the stream around the corners, with the resulting flow distortion affecting the diffusers downstream. The large end of the last diffuser was found stalled on one side, and nearly stalled flow was also found at the tip of the fan. Cumulatively, these adverse flow characteristics were found to reduce the flow quality and the efficiency of the tunnel. Several recommendations are made for further evaluation of techniques intended to correct the observed flow deficiencies.

| 17. Key Words (Suggested by Author(s)) | 18. Distribution Statement |
|---|---|
| Wind tunnel (subsonic)<br>Diffuser flow<br>Duct flow<br>Wind tunnel performance<br>Turning vanes | Unclassified-Unlimited<br><br>Subject Category 02 |

| 19. Security Classif. (of this report) | 20. Security Classif. (of this page) | 21. No. of Pages | 22. Price* |
|---|---|---|---|
| Unclassified | Unclassified | 76 | A05 |



For sale by the National Technical Information Service, Springfield, Virginia 22161

End of Document